



## OPEN ACCESS

## EDITED BY

Michele Giani,  
National Institute of Oceanography and  
Experimental Geophysics, Italy

## REVIEWED BY

Gianmarco Ingrosso,  
National Research Council (CNR), Italy  
Maribel I. García-Ibáñez,  
Spanish National Research Council (ICM-  
CSIC), Spain

## \*CORRESPONDENCE

Agneta Fransson  
✉ agneta.fransson@npolar.no

RECEIVED 31 January 2023

ACCEPTED 16 August 2023

PUBLISHED 20 October 2023

## CITATION

Fransson A, Chierici M, Granskog MA,  
Dodd PA and Stedmon CA (2023) Impacts  
of glacial and sea-ice meltwater, primary  
production, and ocean CO<sub>2</sub> uptake on  
ocean acidification state of waters by the  
79 North Glacier and northeast Greenland  
shelf.

*Front. Mar. Sci.* 10:1155126.

doi: 10.3389/fmars.2023.1155126

## COPYRIGHT

© 2023 Fransson, Chierici, Granskog, Dodd  
and Stedmon. This is an open-access article  
distributed under the terms of the [Creative  
Commons Attribution License \(CC BY\)](#). The  
use, distribution or reproduction in other  
forums is permitted, provided the original  
author(s) and the copyright owner(s) are  
credited and that the original publication in  
this journal is cited, in accordance with  
accepted academic practice. No use,  
distribution or reproduction is permitted  
which does not comply with these terms.

# Impacts of glacial and sea-ice meltwater, primary production, and ocean CO<sub>2</sub> uptake on ocean acidification state of waters by the 79 North Glacier and northeast Greenland shelf

Agneta Fransson<sup>1\*</sup>, Melissa Chierici<sup>2</sup>, Mats A. Granskog<sup>1</sup>,  
Paul A. Dodd<sup>1</sup> and Colin A. Stedmon<sup>3</sup>

<sup>1</sup>Norwegian Polar Institute, Fram Centre, Tromsø, Norway, <sup>2</sup>Institute of Marine Research, Fram Centre, Tromsø, Norway, <sup>3</sup>National Institute for Aquatic Resources, Technical University of Denmark, Kongens Lyngby, Denmark

The waters adjacent to the Nioghalvfjærdsbræ (79 North Glacier, 79NG) are influenced by Greenland Ice Sheet (GrIS) melt, sea-ice meltwater, and waters on the adjacent northeast Greenland shelf (NEGS). We investigated ocean acidification (OA) variables and the role of freshening, primary production, and air-sea CO<sub>2</sub> exchange in Dømmphna Sound (DS) and on the NEGS in the summers of 2012 and 2016. The upper 150 m consisted of Polar Water with Arctic origin that was divided into a fresh surface layer (SL<50 m) and a cold halocline layer (CHL, 50 to 150 m). The layer below 150 m was of Atlantic origin. The SL freshwater was larger in 2012 than in 2016, mainly originated from local 79NG (and GrIS) runoff in DS, whereas on the NEGS in both years, it was mainly from sea-ice melt. The lowest aragonite saturation state ( $\Omega_{Ar}$ ) of 1.13 was found in the SL in 2012. Biological CO<sub>2</sub> drawdown at primary production caused increased  $\Omega_{Ar}$  in SL, which compensated for most of the  $\Omega_{Ar}$  decrease due to the freshwater dilution of carbonate ions reducing total alkalinity, hence preventing corrosive conditions. This was most pronounced near the 79NG front in 2012, where surface stratification was most pronounced coinciding with large glacial meltwater fractions. Freshening decreased  $\Omega_{Ar}$  by 0.4 at the 79NG front was compensated by biological CO<sub>2</sub> drawdown by ~0.5. In 2016, a well-mixed water column in DS and NEGS, with dilution by sea-ice meltwater, caused less compensation on  $\Omega_{Ar}$  by biological CO<sub>2</sub> drawdown than in 2012. In future with changing climate and changing ocean chemistry, the increased meltwater effects may overcome the alleviating effects of biological CO<sub>2</sub> drawdown on OA with unfavorable conditions for calcifying organisms. However, our study also suggests that primary production may be stimulated by stratification from surface meltwater. In addition, Atlantification and subglacial discharge may result in upwelling of inorganic nutrients that could promote primary production.

## KEYWORDS

Dømmphna Sound, Nioghalvfjærdsbræ, Arctic fjord, total alkalinity, biogeochemical processes, polar water, nutrients, aragonite saturation

## 1 Introduction

Substantial thinning, retreat, and melting of the Greenland Ice Sheet (GrIS) and Arctic glaciers have been observed over the last decades (e.g., Rignot et al., 2008; Rignot et al., 2010; Khan et al., 2014) due to climate change, as resulting in changes in the seawater chemical composition and carbonate chemistry (e.g., Meire et al., 2014; Fransson et al., 2015; Henson et al., 2022). Melting of glacier ice by increased presence and warming of the Atlantic water (Atlantification) by marine-terminating glaciers in northeast Greenland fjords have recently been reported (Straneo et al., 2010; de Steur et al., 2014; Gjelstrup et al., 2022), which will further act to accelerate GrIS glacial melting. Dijnphna Sound (DS) is a site of significant meltwater export from the Nioghalvfjædsbræ (79 North Glacier; 79NG; von Albedyll et al., 2021; Figure 1A) and suitable laboratory for the study of the effects of freshening on the marine carbonate system (or CO<sub>2</sub> system).

The carbonate chemistry parameters, including calcium carbonate (CaCO<sub>3</sub>) saturation state ( $\Omega$ ), are key variables to monitor and assess a change in ocean carbonate chemistry and ocean acidification (OA) state.  $\Omega$  provides information about the thermodynamic potential for CaCO<sub>3</sub> shell dissolution. The calcite and aragonite forms of CaCO<sub>3</sub> are biologically produced and are rarely formed inorganically. However, the solubility is chemically controlled and depends on salinity, temperature, pressure, and carbonate ion concentration. Calcite (Ca) is the stable form and aragonite (Ar) is the meta-stable form, which is given by their different solubility products,  $K_{sp}$ . When  $\Omega > 1$ , the mineral will be kept in solid state and when  $\Omega < 1$ , thermodynamic state, the mineral will tend to dissolve, also referred to as corrosive condition for CaCO<sub>3</sub>. The  $\Omega$  value is expressed by the product of concentrations of calcium ([Ca<sup>2+</sup>]) and carbonate ions ([CO<sub>3</sub><sup>2-</sup>]) in seawater divided by the  $K_{sp}$  at a given temperature (T), practical salinity (S), and pressure, according to Equation 1:

$$\Omega = [\text{CO}_3^{2-}]x[\text{Ca}^{2+}]/K_{sp} \quad (1)$$

In the ocean, the [CO<sub>3</sub><sup>2-</sup>] and [Ca<sup>2+</sup>] control much of the variability in  $\Omega_{Ar}$  and susceptibility for dissolution.

Previous studies in the Arctic Ocean and fjords in Spitsbergen and southern Greenland show changes in ocean chemistry with freshening and that it results in lower  $\Omega$ , total alkalinity (AT), and pH<sub>T</sub> referred to as OA (Chierici and Fransson, 2009; Yamamoto-Kawai et al., 2009; Azetsu-Scott et al., 2010; Sejr et al., 2011; Azetsu-Scott et al., 2014; Fransson et al., 2015; Fransson et al., 2016; Ericson et al., 2019a; Fransson et al., 2020; Henson et al., 2022). Decreasing  $\Omega$  and loss in [CO<sub>3</sub><sup>2-</sup>] will cause damage to CaCO<sub>3</sub> shells of calcifying marine organisms, such as aragonite-shell forming pteropods, with potentially detrimental effects on organisms and ecosystem (e.g., Manno et al., 2017; Bednaršek et al., 2021; Niemi et al., 2021). However, living calcifying organisms can produce shells at  $\Omega < 1$  but to an energetic cost and lead to unfavorable conditions (Spalding et al., 2017).

The Arctic Ocean is particularly vulnerable to OA due to the cold and relatively fresh surface waters from meltwater (glacial and sea-ice melt) and river runoff that dissolves more atmospheric CO<sub>2</sub> than saltier

and warmer waters (Chierici and Fransson, 2009). These waters have locally low pH<sub>T</sub> and are naturally low in carbonate ions (CO<sub>3</sub><sup>2-</sup>) and total alkalinity (AT) due to dilution by large freshwater runoff (Fransson et al., 2009; Chierici et al., 2011). Consequently, the Arctic Ocean has the lowest  $\Omega_{Ar}$  compared with the world oceans (e.g., Chierici and Fransson, 2009). Increased freshwater runoff from the GrIS has the potential to further enhance OA both locally in Greenland fjords (e.g., Henson et al., 2022) and on the shelf (e.g., NEGS). On the other hand, studies in Arctic fjords have shown that glacial drainage water from calcareous bedrock can partly mitigate the effect of freshening due to addition of buffering ions such as [CO<sub>3</sub><sup>2-</sup>] (Sejr et al., 2011; Fransson et al., 2015; Fransson et al., 2020). Moreover, sea ice can also contribute with [CO<sub>3</sub><sup>2-</sup>] during the dissolution of sea-ice-derived CaCO<sub>3</sub> (ikaite) (Rysgaard et al., 2012; Fransson et al., 2015; Fransson et al., 2020).

Primary production (PP) results in increased  $\Omega_{Ar}$  and pH<sub>T</sub> due to CO<sub>2</sub> (DIC) drawdown in spring/summer, net respiration (i.e., CO<sub>2</sub> production) decreases  $\Omega_{Ar}$  and pH<sub>T</sub> in fall/winter, and freshwater supply generally lowers  $\Omega_{Ar}$  and pH<sub>T</sub> through dilution of ions (Chierici and Fransson, 2018). Primary and secondary production in glacier influenced fjords can be stimulated by meltwater-driven upwelling of nutrient-rich subglacial water (Apollonio, 1973; Sejr et al., 2011; Lydersen et al., 2014; Meire et al., 2014; Fransson et al., 2015; Halbach et al., 2019) and addition of micronutrients (e.g., iron; Bhatia et al., 2013; Hopwood et al., 2020; Krisch et al., 2021). Moreover, deeper waters that have been isolated from the surface and accumulated CO<sub>2</sub> from organic matter degradation can be entrained and further decrease  $\Omega$  and pH<sub>T</sub> (Henson et al., 2022).

Observations of carbonate chemistry in the northern Greenland fjords are scarce due to limited accessibility. Here, we focus on the water column carbonate chemistry, inorganic nutrients, and OA state in 2 years in DS and NEGS, next to the 79NG (Figure 1A). Estimates and evaluation of drivers affecting the carbonate chemistry, OA, and potential for air-sea CO<sub>2</sub> exchange in the upper 50 m in the DS and NEGS are presented and discussed for the two summers/years, in relation to freshening and climate change.

## 2 Study area

The DS and NEGS system are one of the largest outlets of the northeast Greenland ice stream (NEGIS), extending more than 600 km into the interior of the GrIS and draining 9% of it (Figure 1B; Thomsen et al., 1997; Joughin et al., 2001; Khan et al., 2014). The 79NG is a marine-terminating glacier with two calving fronts and is connected to GrIS (Figures 1A, B). One front is located south of Hovgaard Island and is 30–35 km wide. A second front (Spaltegletscher) calves into the 10-km-wide DS (e.g., Thomsen et al., 1997; Mayer et al., 2000; Khan et al., 2014), which is the focus of this study (Figures 1A, B). The floating part of the 79NG ice tongue shows strong surface melting during summer with an annual ablation of 1 m (Thomsen et al., 1997). The DS is around 60–70 km long from near the sill (at 130 m) to the 79NG front at the fjord head. The upper 150 m is the Polar Water (PW; Gjelstrup et al., 2022), which in this study is divided into two layers; the

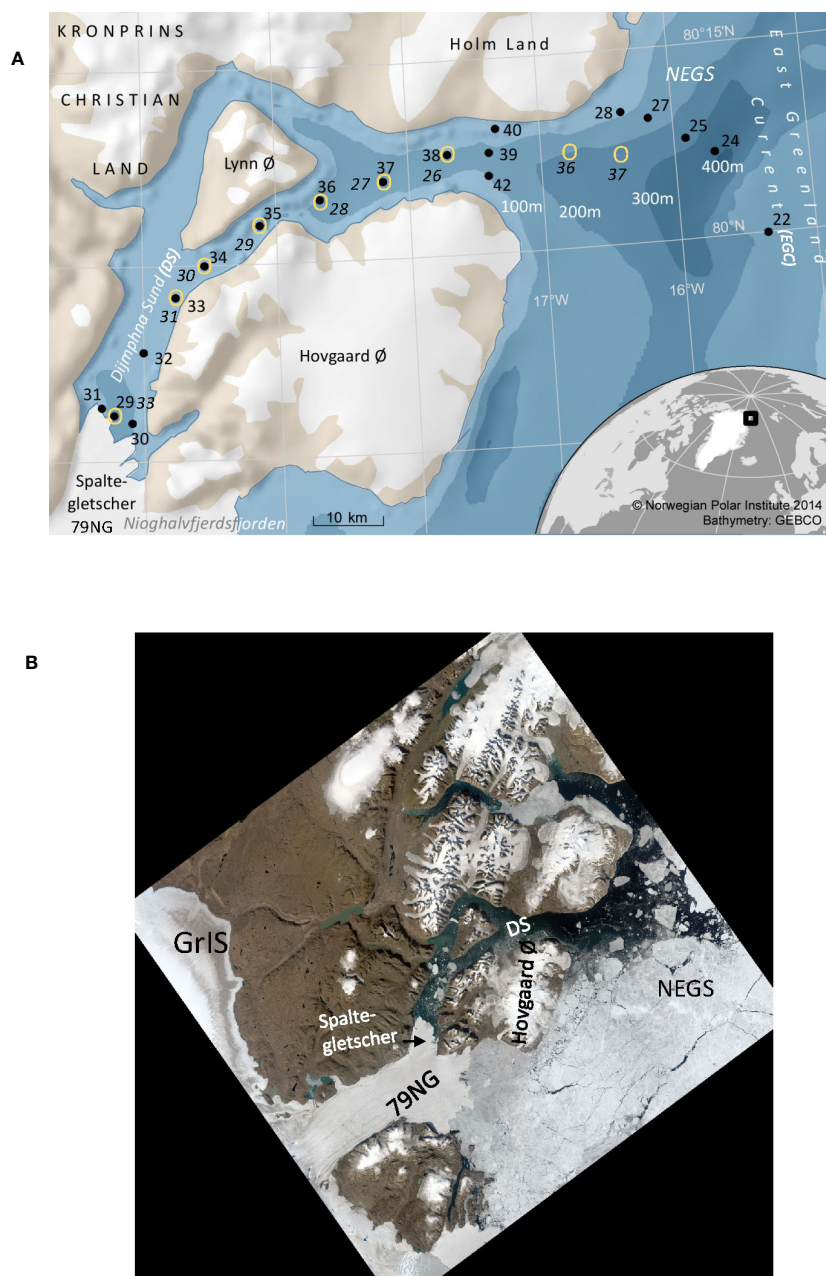


FIGURE 1

(A) Map of study area and location of stations collected in the Dijnphna Sound (DS), the glacier front of Spaltegletscher (a branch of the 79°N North Glacier, 79NG) and on the adjacent Northeast Greenland shelf (NEGS) in 27–28/08/2012 (black dots) and 3–4/09/2016 (yellow circles). Station numbers in 2012 (black) and 2016 (black italic font) and in 2012 stations #39, #40, and #42 in 2012 were located at the sill of DS. In 2016, there was no sampling at the sill. Bathymetry is shown in different shades of blue, and white numbers represent the depth of the contour in meters. White areas on land are glaciers. (B) Aerial view from satellite (Landsat image courtesy of the U.S. Geological Survey) of the area adjacent to the 79NG in August 2012 including Dijnphna Sound (DS), Northeast Greenland shelf (NEGS), and Greenland Ice Sheet (GrIS). The picture also shows the bedrock (brown area) and sea ice (white) on the adjacent shelf. The DS was mainly open and interspersed with occasional ice bergs (white squares).

relatively fresh surface layer affected by seasonal processes such as primary production, meltwater, and seasonal warming (SL; 0 to <50 m), and a cold halocline layer (CHL; >50–150 m) at near-freezing temperatures ( $\theta < 0^{\circ}\text{C}$ ) with a salinity of approximately 32.5 (Figure 2A). The SL is mainly formed locally and is affected by glacial meltwater (Thomsen et al., 1997). The layer below 150 m to bottom consists of water of Atlantic origin (AW;  $S > 34.4$ ,  $\theta > 0^{\circ}\text{C}$ ; Gjelstrup et al., 2022).

## 3 Materials and methods

### 3.1 Sampling and analytical methods

Sampling in the DS and NEGS was performed in 27–28/08/2012 and 3–4/09/2016 onboard *R/V Lance*, as part of the Norwegian Polar Institute's long-term monitoring in the area. The station locations are presented in Table 1 and Figure 1A. In our study,

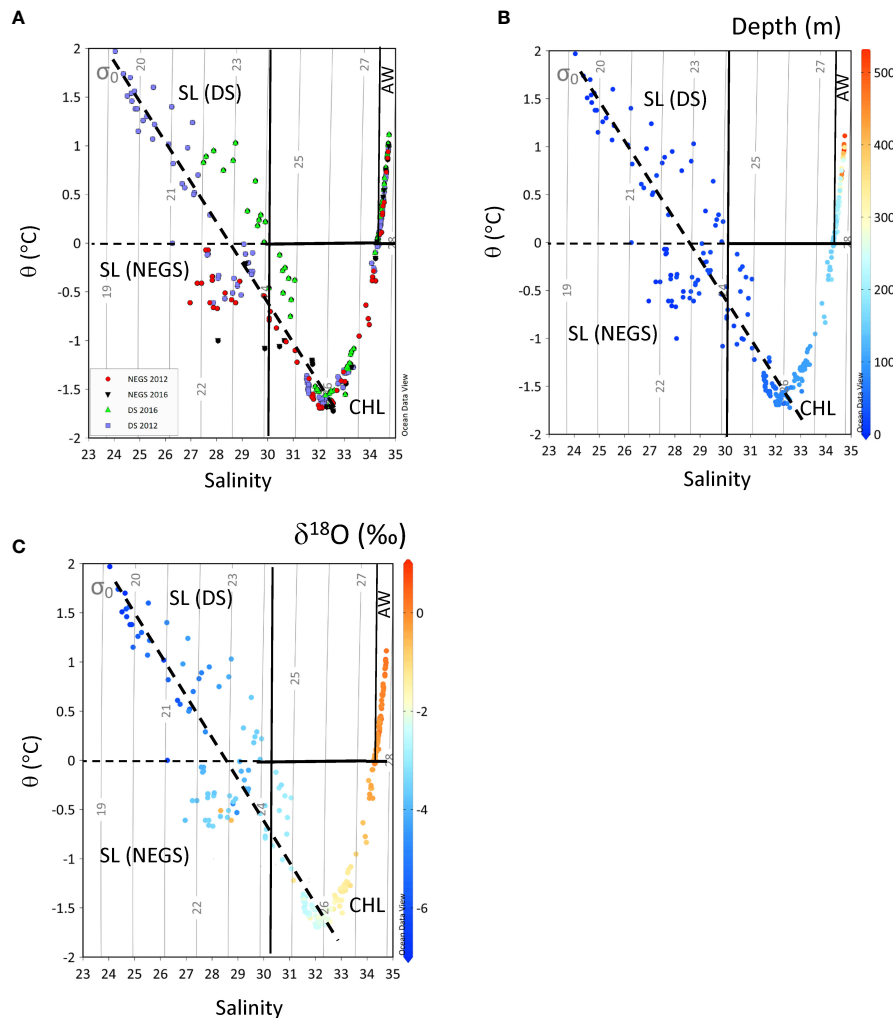


FIGURE 2

Potential temperature ( $\theta$ , y-axis,  $^{\circ}\text{C}$ ) against practical salinity ( $S$ , x-axis) for (A) Dijnphna Sound (DS) in 2012 (purple squares) and in 2016 (light-green triangle), the Northeast Greenland shelf (NEGS) in 2012 (red filled circles) and in 2016 (black filled inverted triangle). (B) Depth (m, z-axis) and (C)  $\delta^{18}\text{O}$  (‰, z-axis), in 2012 and 2016, respectively. The light-gray contours show the density ( $\sigma_{\theta}$ ) at zero-reference pressure  $\sigma_{\theta}$ , ( $\text{kg m}^{-3}$ ). The mixing line (dashed black line) shows the dilution line from cold halocline layer (CHL) to the surface layer (SL). Water masses are divided into SL in DS and on the NEGS, CHL, and the Atlantic water (AW) according to properties after Gjelstrup et al. (2022).

summer data from DS and 40 km to the east from the sill of DS represent water on the adjacent NEGS (Figure 1A). Abbreviations throughout the manuscript are summarized in a glossary table (Table S1).

Water samples were collected from 8-L Niskin bottles mounted on a General Oceanics 12-bottle rosette equipped with a conductivity–temperature–depth sensor (CTD, Sea-Bird SBE 911plus) and a chlorophyll a fluorescence probe (WetLabs). Water samples were collected (at fixed depths) from the same Niskin bottles for analysis of salinity, water oxygen isotopic ratio ( $\delta^{18}\text{O}$ - $\text{H}_2\text{O}$ , hereafter referred to as  $\delta^{18}\text{O}$ ), dissolved inorganic nutrients, and the carbonate system parameters total inorganic carbon (DIC) and total alkalinity (AT).

Samples for the analyses of DIC and AT were collected in 250-mL borosilicate bottles following standard sampling protocols (Dickson et al., 2007). Samples for AT and DIC were unfiltered. Upon collection, samples were stored in the dark at  $4^{\circ}\text{C}$  until

analysis onboard within 5 to 12 h, so no preservative  $\text{HgCl}_2$  was needed. In 2012 and 2016, DIC was determined onboard by coulometric titration (Johnson et al., 1985) using a Versatile Instrument for the Determination of Total inorganic carbon and titration Alkalinity (VINDTA 3C, Marianda, Germany) and AT using potentiometric titration with 0.05 M HCl acid and NaCl ( $35 \text{ g L}^{-1}$ ), to have similar ion strength as the samples, on a Metrohm titration system following the methods described by Mattsdotter-Björk et al. (2014) and Dickson et al. (2007). Additional seawater samples were taken for post-cruise analyses for AT using a Versatile Instrument for the Determination of Titration Alkalinity (VINDTA 3S, Marianda, Germany). The precision was  $\pm 2 \mu\text{mol kg}^{-1}$  for AT and  $\pm 2 \mu\text{mol kg}^{-1}$  for DIC, based on replicates of Certified Reference Material (CRM) regardless of instrumentation. The accuracies of AT and DIC were controlled against CRM (batch no. 117) supplied by A. Dickson (San Diego, USA) by applying a correction factor to the measured values based on the ratio between

TABLE 1A Date, location and bottom depth for stations used in the study from 2012 in the fjord of Dijnphna Sound (DS), NE Greenland shelf (NEGS).

Station #	Date mm/dd/yyyy	Latitude (°N)	Longitude (°W)	Bottom depth (m)	Location
22	08/27/2012	80.00	-15.36	245	NEGS
24	08/27/2012	80.11	-15.70	431	NEGS
25	08/27/2012	80.13	-15.91	217	NEGS
27	08/27/2012	80.16	-16.18	352	NEGS
28	08/27/2012	80.17	-16.38	152	NEGS
29*	08/27/2012	79.81	-20.22	538	DS (79NG)
30	08/28/2012	79.80	-20.09	215	DS (79NG)
31	08/28/2012	79.82	-20.31	327	DS (79NG)
32	08/28/2012	79.89	-20.00	321	DS
33*	08/28/2012	79.96	-19.76	394	DS
34*	08/28/2012	80.00	-19.54	533	DS
35*	08/28/2012	80.05	-19.12	467	DS
36*	08/28/2012	80.08	-18.67	239	DS
37*	08/28/2012	80.10	-18.19	202	DS
38*	08/28/2012	80.13	-17.70	214	DS
39	08/28/2012	80.13	-17.39	156	sill
40	08/28/2012	80.16	-17.33	179	Sill
42	08/28/2012	80.10	-17.40	105	Sill

Stations located near the 79NG glacier front is denoted 79NG. Stations denoted with an asterisk (\*) indicate the seven stations that were repeated in 2016 (see also Table 1B).

TABLE 1B Date, location and bottom depth for stations used in the study from 2016 in the fjord of Dijnphna Sound DS, NE Greenland shelf NEGS.

Station #	Date mm/dd/yyyy	Latitude (°N)	Longitude (°W)	Bottom depth (m)	Location
26*	09/03/2016	80.13	-17.71	217	Sill
27*	09/03/2016	80.10	-18.20	192	in DS
28*	09/04/2016	80.08	-18.66	244	in DS
29*	09/04/2016	80.05	-19.11	462	in DS
30*	09/04/2016	79.99	-19.53	513	in DS
31*	09/04/2016	79.97	-19.76	493	in DS
33*	09/04/2016	79.81	-20.22	530	DS (79NG)
36	09/04/2016	80.13	-16.95	249	NEGS
37	09/04/2016	80.11	-16.24	354	NEGS

Stations located near the 79NG glacier front is denoted 79NG. Stations denoted by asterisk (\*) indicate the repeat stations from 2012.

the certified value and the measured CRM values. The correction factors were  $1.001 \pm 0.002$  and  $1.060 \pm 0.002$  for AT and DIC, respectively.

The samples for determination of inorganic nutrients (nitrate, phosphate, silicic acid) were collected in acid-washed polyethylene bottles and frozen at  $-20^{\circ}\text{C}$  until laboratory analyses using an autoanalyzer (Skalar) following the approach of Hansen and Koroleff (1999). The detection limit was  $0.06 \text{ mmol m}^{-3}$  for phosphate ( $[\text{PO}_4^{3-}]$ ),  $0.2 \text{ mmol m}^{-3}$  for nitrate ( $[\text{NO}_3^-]$ ) (only in

2012), and  $0.3 \text{ mmol m}^{-3}$  for silicic acid ( $[\text{Si}(\text{OH})_4]$ ) concentrations. In 2016, parts of the nitrate data had large uncertainty ( $>3\sigma$ ), which are not included in the manuscript.  $\delta^{18}\text{O}$  samples were collected in 40-mL glass vials. Upon sample collection, vials were tightly closed and sealed with Parafilm<sup>®</sup>. Measurements in 2012 were done ashore at the G.G. Hatch Stable Isotope Laboratory (University of Ottawa, Canada) using isotope ratio mass spectrometry and Vienna Standard Mean Ocean Water (V-SMOW). The analytical precision was  $\pm 0.05\text{‰}$  (Epstein and Mayeda, 1953). In 2016,  $\delta^{18}\text{O}$

was measured at National Environment Research Council Isotope Geosciences Facility at the British Geological Survey (Keyworth, UK) using a dual-inlet mass spectrometer. Analytical reproducibility was <0.05‰ based on duplicate analyses against V-SMOW. Salinity (on the practical salinity scale, dimensionless) samples were measured onboard using an Autosal<sup>®</sup> salinometer (Dauphinee and Klein, 1975) with the precision of ±0.003 (Dodd et al., 2012).

## 3.2 Calculations

### 3.2.1 Carbonate chemistry

The concentrations of AT and DIC, inorganic nutrients (phosphate and silicic acid), salinity, and temperature were used as input parameters in a CO<sub>2</sub>-chemical speciation model (CO2SYS program, Pierrot et al., 2006) to calculate the full carbonate system including *in situ* pH<sub>T</sub>, *f*CO<sub>2</sub>, [CO<sub>3</sub><sup>2-</sup>], Ω<sub>Ca</sub>, and Ω<sub>Ar</sub>. The calculations were performed using the total hydrogen ion scale and the hydrogen sulfate ([HSO<sub>4</sub><sup>-</sup>]) dissociation constant of Dickson (1990). We used the carbonate system dissolution constants from Mehrbach et al. (1973) refit by Dickson and Millero (1987). The solubility constants for CaCO<sub>3</sub> are estimated according to Mucci (1983), where [Ca<sup>2+</sup>] is proportional to the salinity (10.28 × S/35 μmol kg<sup>-1</sup>). The carbonate system constants were chosen for comparison of Ω<sub>Ar</sub> between previous values in the same region. However, studies have shown that there may be other constants that are more suitable for the colder and lower-salinity water found in this study. Ultimately, the choice of constants relies on several factors such as the input pair (here AT and DIC), the target variable (here Ω<sub>Ar</sub>), the research question, and the seawater properties as demonstrated in many intercomparison studies (e.g., Chierici et al., 2004; Orr et al., 2018; Sulpis et al., 2020). Orr et al. (2018) found that a pair of AT and DIC gave the lowest combined standard uncertainty in the calculated [CO<sub>3</sub><sup>2-</sup>], which resulted in a corresponding uncertainty of ±0.0286 in the calculated Ω<sub>Ar</sub> in the CO2SYS excel version. The estimate of the temperature and salinity dependence of the constants (K1 and K2) for carbonic acids should be suitable for the polar water properties. For example, for fresher and colder (T<0°C) polar water, the constants of Roy et al. (1993) were shown to be more suitable (Chierici and Fransson, 2009). Orr et al. (2018) also demonstrated that most of the uncertainty is related to K1 when *f*CO<sub>2</sub> is the target variable and in K2 for estimates of Ω<sub>Ar</sub>. This is due to the smaller temperature dependence in Ω<sub>Ar</sub> than for gas solubility (e.g., *f*CO<sub>2</sub>) (Orr et al., 2018; Sulpis et al., 2020). These types of studies are normally performed by internal consistency using three sets of measured carbonate system variables, for example, AT, DIC, and pH<sub>T</sub> (Chierici and Fransson, 2009). To overcome the lack of a third carbonate system variable in this study, we investigated the difference (ΔΩ<sub>Ar</sub><sub>MEAS-L</sub>) between Ω<sub>Ar</sub> calculated from Lueker et al. (2000) (Ω<sub>Ar</sub><sub>L</sub>) and the ones used here (ΔΩ<sub>Ar</sub><sub>MEAS</sub>) based on Dickson and Millero (1987) (Figure S1A). The mean and standard deviation of ΔΩ<sub>Ar</sub><sub>MEAS-L</sub> was -0.004 ± 0.001, ranging between -0.006 and -0.002 (Figure S1B). The largest ΔΩ<sub>Ar</sub><sub>MEAS-L</sub> of -0.006 was found at -1.5°C (Figure S1B). This uncertainty is of the same

magnitude as the uncertainty in Ω<sub>Ar</sub> derived from the analytical precision in AT and DIC of ±0.001 and one magnitude smaller (third decimal) than the findings in Orr et al. (2018), hence having an insignificant impact on the results.

### 3.2.2 Freshwater fractions and endmembers

To investigate the local effects of freshwater addition on Ω<sub>Ar</sub>, the freshwater content (meteoric and sea-ice meltwater) (FW<sub>TOT</sub>) was calculated based on a reference (REF) seawater (SW<sub>REF</sub>) located at the boundary between SL and CHL with a salinity (S<sub>REF</sub>) of 32.5, at 50 m, and the measured salinity of the water sample (S<sub>MEAS</sub>).

$$FW_{TOT} = 1 - S_{MEAS}/S_{REF} \quad (2)$$

AT, S, and T were used to investigate the freshwater endmembers. Linear regressions of AT vs. S for the different water layers give the AT freshwater endmember (AT<sub>FWEM</sub>) at the intercept at zero (y-axis) salinity, for SL and CHL in the DS and the NEGS.

Fractions of meteoric water (F<sub>GM</sub>) and sea-ice meltwater (F<sub>SIM</sub>) were estimated in the SL using the relationships between salinity and δ<sup>18</sup>O, and endmember values for glacial meltwater in the SL (GM), sea-ice meltwater (SIM), and SW<sub>REF</sub> (Table 2), following Equations 3–5 (Macdonald et al., 1999; Chierici et al., 2011).

$$1 = F_{REF} + F_{GM} + F_{SIM} \quad (3)$$

$$S = S_{REF}F_{REF} + S_{SIM}F_{SIM} \quad (4)$$

$$\delta^{18}O = \delta^{18}O_{REF}F_{REF} + \delta^{18}O_{GM}F_{GM} + \delta^{18}O_{SIM}F_{SIM} \quad (5)$$

### 3.2.3 Effects of freshwater and primary production on saturation state

The impact of freshening (ΔX<sub>FW</sub>) and inorganic carbon drawdown by PP (ΔX<sub>BIO</sub>) on concentrations of DIC, AT, and PO<sub>4</sub><sup>3-</sup> (depicted as X here) was partitioned using the approach described in Fransson et al. (2001); Fransson et al. (2004), where the reference concentrations (X<sub>REF</sub>) were assumed not to be affected by summer freshening and PP. First, ΔX<sub>FW</sub> was estimated by multiplying FW<sub>TOT</sub> for each sample in the upper 50 m with the AT, DIC, and PO<sub>4</sub><sup>3-</sup> in the SW<sub>REF</sub> (X<sub>REF</sub>) according to Equation 6. Secondly, freshwater-corrected X was calculated by subtracting ΔX<sub>FW</sub> with X<sub>REF</sub> (Equation 7). These X<sub>FW</sub> values were used in CO2SYS (Section 3.2.1) to calculate freshwater corrected Ω<sub>Ar</sub> (Ω<sub>Ar</sub><sub>FW</sub>).

TABLE 2 End-member parameter values for salinity and δ<sup>18</sup>O for sea-ice meltwater (SIM), glacial meltwater (GM) and reference seawater (SW<sub>REF</sub>). SW<sub>REF</sub> values were from this study.

	Salinity	δ <sup>18</sup> O (‰)
Sea-ice meltwater (SIM)	2.3±1.1	-1.0±0.6
Glacial meltwater (GM)	0	-28±3
Reference seawater (SW <sub>REF</sub> )	32.5±0.8	-2.5±0.7

SIM from melted sea ice in western Fram Strait (Fransson and Chierici, 2023), and GM from values were from Carlson et al. (2019).

$$\Delta X_{FW} = X_{REF} \times FW_{TOT} \quad (6)$$

$$X_{FW} = X_{REF} - \Delta X_{FW} \quad (7)$$

$X_{BIO}$  and  $\Delta X_{BIO}$  were calculated using the change in  $[PO_4^{3-}]$  converted to carbon drawdown ( $\Delta DIC_{BIO}$ ) using Redfield (Redfield et al., 1963) stoichiometry C:P = 106/1 (Equation 8A, 8B) as a proxy for PP.  $[PO_4^{3-}]$  was used to avoid potential artefacts resulting from external nitrogen sources such as atmospheric nitrogen deposition. The variability in C:P ratios and consequences for the  $DIC_{BIO}$  are discussed (see Section 5.2).

$$\Delta DIC_{BIO} = \Delta [PO_4^{3-}] \times 106 \quad (8A)$$

$$X_{BIO} = X_{REF} - \Delta X_{BIO} \quad (8B)$$

The AT values are affected only to a minor extent by PP. However, by the assimilation of  $NO_3^-$  and hydrogen ions for the formation of protein during photosynthesis, the AT increases and was corrected by  $1 \mu mol kg^{-1}$  per one unit of  $NO_3^-$  change ( $AT_{BIO}$ ).  $AT_{BIO}$  and  $DIC_{BIO}$  were used as input variables CO2SYS (Section 3.2.1) to obtain values of  $\Omega_{Ar}$  and other carbonate system parameters that were affected only by biological  $CO_2$  drawdown ( $\Omega_{ArBIO}$ ) as for  $\Omega_{ArFW}$ . The resulting net effects on  $\Omega_{Ar}$  of either freshwater addition ( $\Delta \Omega_{ArFW}$ ) or biological  $CO_2$  drawdown ( $\Delta \Omega_{ArBIO}$ ) in the DS and on the NEGS were estimated as the difference between  $\Omega_{Ar}$  in the  $SW_{REF}$  ( $\Omega_{ArREF}$ ) and the  $\Omega_{ArFW}$  and  $\Omega_{ArBIO}$ , respectively (Equation 9A, 9B, 9C).

$$DIC_{BIO} = DIC_{REF} - \Delta DIC_{BIO} \quad (9A)$$

$$DIC_{FW} = DIC_{REF} - \Delta DIC_{FW} \quad (9B)$$

$$AT_{FW} = AT_{REF} - \Delta AT_{FW} \quad (9C)$$

To investigate the role of other processes ( $\Delta X_{DIFF}$ ,  $\Delta X_{BIO}$  and  $\Delta X_{FW}$ ) were subtracted from the  $DIC_{REF}$  and  $AT_{REF}$  to obtain  $X_{CORR}$  (Equation 10), which was compared with the measured AT and DIC ( $X_{MEAS}$ ) according to Equation 11. A positive  $\Delta X_{DIFF}$  suggests a net addition of  $[CO_3^{2-}]$  possibly from the contribution of bedrock-derived carbonic minerals in the glacial drainage water.

$$X_{CORR} = X_{REF} - \Delta X_{BIO} - \Delta X_{FW} \quad (10)$$

$$\Delta X_{DIFF} = X_{MEAS} - X_{CORR} \quad (11)$$

$$\Delta X_{GLAC} = FW_{TOT} \times X_{GLAC} \quad (12)$$

where  $X_{GLAC}$  is the concentration of AT at zero S (i.e., intercept) in the linear regression between AT and S.  $\Delta AT_{GLAC}$  is the change due to effects of glacial drainage water. The supply of  $[CO_3^{2-}]$  results in AT changes with 1 mol and DIC with 2 mol.  $\Delta DIC_{REST}$  is the residual (Equation 13), which consists of processes that are not considered in Equations 9 to 12, such as air-sea  $CO_2$  exchange.

$$\Delta DIC_{REST} = \Delta DIC_{DIFF} - \Delta AT_{GLAC}/2 \quad (13)$$

All calculated variables derived from Equations 11 to 13 were depth-integrated (trapezoid) in the SL.

### 3.2.4 Calculations of $N^*$

The semiconservative tracer  $N^*$  ( $mmol m^{-3}$ ) identifies deviations from conservative behavior between nitrogen and  $PO_4^{3-}$  concentrations according to Equation 14 (Deutsch et al., 2001). A deficit in  $NO_3^-$  relative to  $PO_4^{3-}$  is a signature of denitrification or anammox and results in negative  $N^*$  values. On the Arctic shelves, the CHL is influenced by mineralization of organic matter close to surface sediments at low oxygen (and low  $pH_T$ , high  $CO_2$ ) conditions, which imparts a negative  $N^*$  signature to this layer (Anderson et al., 2013). This can be used to trace the CHL originating from the Arctic Ocean and shelves.

$$N^* = NO_3^- - 16 \times PO_4^{3-} + 2.9 \quad (14)$$

## 4 Results

### 4.1 Physical and chemical properties

In 2012, the salinity of the SL was the lowest, extending down to a salinity of around 24, whereas the lowest salinity in SL in 2016 was around 27 (Figure 2A). The warmest and freshest SL was found in DS in 2012 (Figure 2B). This coincided with the lowest  $\delta^{18}O$  values of less than  $-6\text{‰}$  (Figure 2C). In 2012, the CHL, the potential temperature ( $\theta$ ), and salinity properties were generally similar between the NEGS and the DS. However, the minimum  $\theta$  was observed on the NEGS in 2016, whereas the DS was warmer in the DS in the same year (Figures 2A, B).  $\delta^{18}O$  values also clearly differed between the water layers, where the lowest  $\delta^{18}O$  was found in the SL in 2012 (Figure 2C), increasing to the CHL with  $\delta^{18}O$  values between  $-3$  and  $-1\text{‰}$ . The AW contained the largest  $\delta^{18}O$  values ( $\sim 0.5\text{‰}$ ) and was similar in both years and areas (Figure 2C).

Vertical and horizontal patterns in the variables were similar between the 2 years except for more distinct gradients in the SL in 2012 (Figures 3A-F). The effect of summer warming and freshening in SL was largest in 2012 ( $T = +2^\circ C$ ) and extended down to 40 m at the 79NG front (Figures 3A, C). Below the SL, the CHL had near-freezing temperatures ( $T < 0^\circ C$ ) with a salinity of approximately 32.5 in both 2012 and 2016 (Figures 3C, D). Below CHL, relatively high S and T water extended to the bottom, which indicated the influence of AW (Figures 3A-D).  $\delta^{18}O$  values increased with depth, and toward the sill ( $-0.4\text{‰}$ ) to the NEGS, and varied between the 2 years, with lowest values near the 79NG front down to  $-8.6\text{‰}$  and  $-5\text{‰}$  in 2012 and 2016, respectively (Figures 3E, F and Table S1).

$[NO_3^-]$  was depleted in the SL and  $[PO_4^{3-}]$  varied between near depletion and  $0.63 \text{ mmol m}^{-3}$  and  $[Si(OH)_4]$  varied between near depletion and  $2 \text{ mmol m}^{-3}$  in both years near the 79NG front and the outer (stations) of DS and NEGS (Figures 3G-L and Table S1). Maximum concentrations of  $[NO_3^-]$  and  $[PO_4^{3-}]$  of  $13 \text{ mmol m}^{-3}$  and  $1 \text{ mmol m}^{-3}$ , respectively, were found in the AW in DS and NEGS (Figures 3G, H and Table S1).

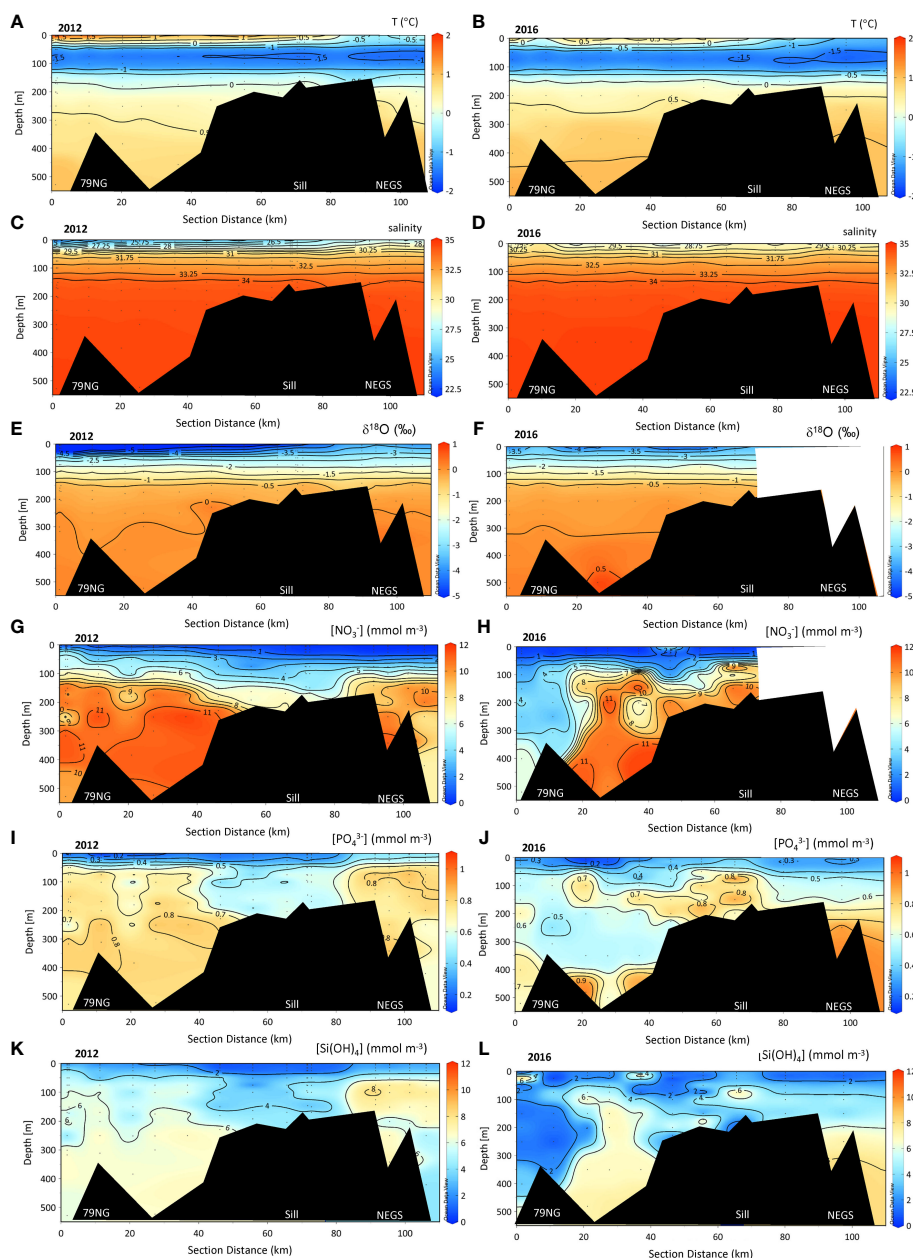


**FIGURE 3**  
Section plots in the water column of temperature ( $T$ ,  $^{\circ}\text{C}$ ), practical salinity ( $S$ ),  $\delta^{18}\text{O}$  (‰), nitrate ( $[\text{NO}_3^-]$ ),  $\text{mmol m}^{-3}$ , phosphate ( $[\text{PO}_4^{3-}]$ ),  $\text{mmol m}^{-3}$ , and silicic acid ( $[\text{Si}(\text{OH})_4]$ ),  $\text{mmol m}^{-3}$ , z-axis concentrations from the 79NG front (distance 0 km) in Dijnphna Sound (DS) to the Northeast Greenland shelf (NEGS) in 2012 (A, C, E, G, I, K) and 2016 (B, D, F, H, J, L). The white shaded area in (F) and (H) indicates no data. The bottom depths at stations near the sill (2012: #39, 40, 42, 2016: #26) were between 105 and 159 m and located between 60 to 70 km from the glacier front (79NG front).

AT and DIC values were lowest in the SL, gradually increasing with depth (Figures 4A–D). The lowest AT and DIC values in both years were observed near the 79NG front, increasing toward the sill and NEGS (Figures 4A–D and Table S1). Large DIC values  $>2,160 \mu\text{mol kg}^{-1}$  were observed below 200 m to the bottom in the DS and on the NEGS, most evident in 2016 (Figure 4D). In both years,  $f\text{CO}_2$  was undersaturated relative to atmospheric values ( $\sim 415 \mu\text{atm}$ , Ny-Ålesund Zeppelin station) in the whole water column (Figures 4E, F). In 2012, the lowest  $f\text{CO}_2$  of  $138 \mu\text{atm}$  was found in the SL at the 79NG front compared with the lowest  $f\text{CO}_2$  of  $269 \mu\text{atm}$  in 2016 in SL (Figures 4E,

F, Table S1). Generally, the surface  $f\text{CO}_2$  increased from the 79NG front toward the sill and further onto the NEGS, especially in 2012. The large differences in  $f\text{CO}_2$  were also reflected in the variability of  $\text{pH}_T$ , where the highest  $\text{pH}_T$  of 8.37 was observed in 2012 by the 79NG front and the corresponding  $\text{pH}_T$  in 2016 of 8.16 (Figures 4G, H and Table S1).

The  $\Omega_{\text{Ar}}$  values (Figures 4I, J) and  $\Omega_{\text{Ca}}$  (i.e., calcite, Table S1, around one unit higher relative to  $\Omega_{\text{Ar}}$ ) were highest in the relatively fresh surface at the 79NG front in both years, particularly evident in 2012 (Figure 4J and Table S1). In 2012,  $\Omega_{\text{Ar}}$  varied in the water

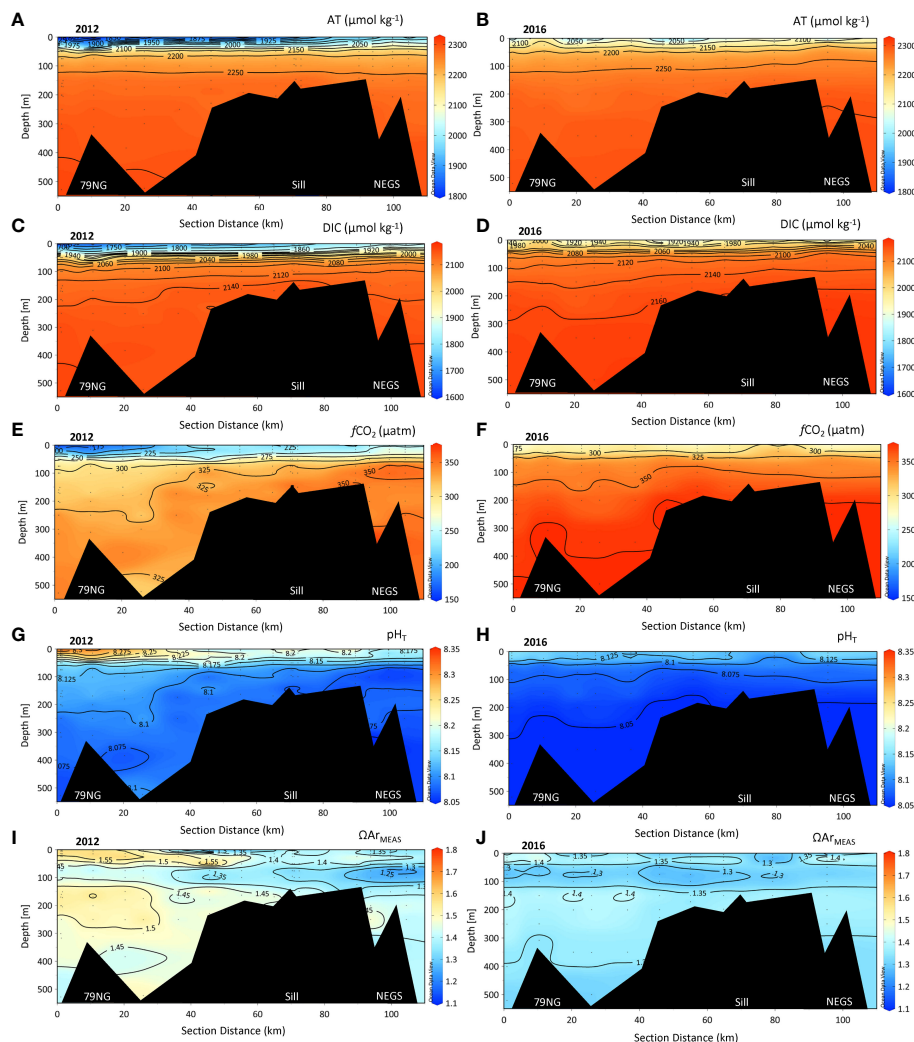


FIGURE 4

Section plots of chemical parameters in the water column of total alkalinity (AT,  $\mu\text{mol kg}^{-1}$ ), total dissolved inorganic carbon (DIC,  $\mu\text{mol kg}^{-1}$ ),  $\text{pH}_T$ , fugacity of carbon dioxide ( $f\text{CO}_2$ ,  $\mu\text{atm}$ ), and aragonite saturation ( $\Omega_{\text{ArMEAS}}$ ), from the 79NG front (distance 0 km) in Dijnphna Sound (DS) to the Northeast Greenland shelf (NEGS) in 2012 (A, C, E, G, I) and 2016 (B, D, F, H, J). The bottom depths at stations near the sill (2012: #39, 40, 42, 2016: #26) were between 105 and 159 m and located between 60 and 70 km from the glacier front (79NG front).

column between 1.13 in DS and 1.75 in the SL near the 79NG. In the SL on the NEGS,  $\Omega_{\text{Ar}}$  was 1.22–1.53 (Figure 4I and Table S1). In 2016,  $\Omega_{\text{Ar}}$  varied less throughout the water column than in 2012 and ranged between 1.23 and 1.44 (Figure 4J and Table S1). The CHL had the lowest  $\Omega_{\text{Ar}}$  values ( $<1.15$ ) in the DS and at the 79NG front and were similar in both years (Figure 4).

## 4.2 Freshwater fractions and alkalinity endmembers

There was a large difference in  $F_{\text{GM}}$  and  $F_{\text{SIM}}$  in SL between the 2 years (Figures 5A–D). In 2012, the largest  $F_{\text{GM}}$  ( $>0.2$ ) was found at the 79NG front and was insignificant on the NEGS (Figure 5A).  $F_{\text{SIM}}$  was largest at the outer DS and on the NEGS ( $F_{\text{SIM}} >0.1$ , Figure 5C). In 2016,  $F_{\text{GM}}$  was lower than 0.1 (Figure 5B) and  $F_{\text{SIM}}$  was  $<0.06$  (Figure 5D).

In SL in DS in 2012 and 2016, the  $\text{AT}_{\text{FWEM}}$  values were  $467 \pm 18 \mu\text{mol kg}^{-1}$  ( $n = 48$ ) and  $411 \pm 14 \mu\text{mol kg}^{-1}$  ( $n = 30$ ), respectively (Figure 6A). On the NEGS,  $\text{AT}_{\text{FWEM}}$  in SL in both years (not shown) were lower than in DS, with an  $\text{AT}_{\text{FWEM}}$  of  $299 \pm 15 \mu\text{mol kg}^{-1}$  in 2012 ( $n = 29$ ) and  $336 \pm 12 \mu\text{mol kg}^{-1}$  ( $n = 8$ ) in 2016. The  $\text{AT}_{\text{FWEM}}$  2016 values on the NEGS were based on eight values so they should be taken with caution.

The  $\text{AT}_{\text{FWEM}}$  values were  $1,338 \pm 6 \mu\text{mol kg}^{-1}$  ( $n = 33$ ) and  $1,555 \pm 6 \mu\text{mol kg}^{-1}$  ( $n = 24$ ) in 2012 and 2016, correspondingly, in the CHL in DS. On the NEGS, the CHL  $\text{AT}_{\text{FWEM}}$  were  $1,361 \pm 6 \mu\text{mol kg}^{-1}$  (in 2012,  $n = 21$ ) and  $1,686 \pm 3 \mu\text{mol kg}^{-1}$  (in 2016,  $n = 6$ ), hence higher in 2016 but estimated with limited number of data points, which may bias the  $\text{AT}_{\text{FWEM}}$  estimate.

$N^*$  in SL and in the AW was positive and negative in the CHL (Figure 6B). The most negative  $N^*$  of  $-10 \mu\text{mol L}^{-1}$  coincided with the highest  $\text{CO}_2$  concentration ( $>24 \mu\text{mol kg}^{-1}$ ) observed in the CHL, most pronounced on the NEGS (Figure 6B). This indicates

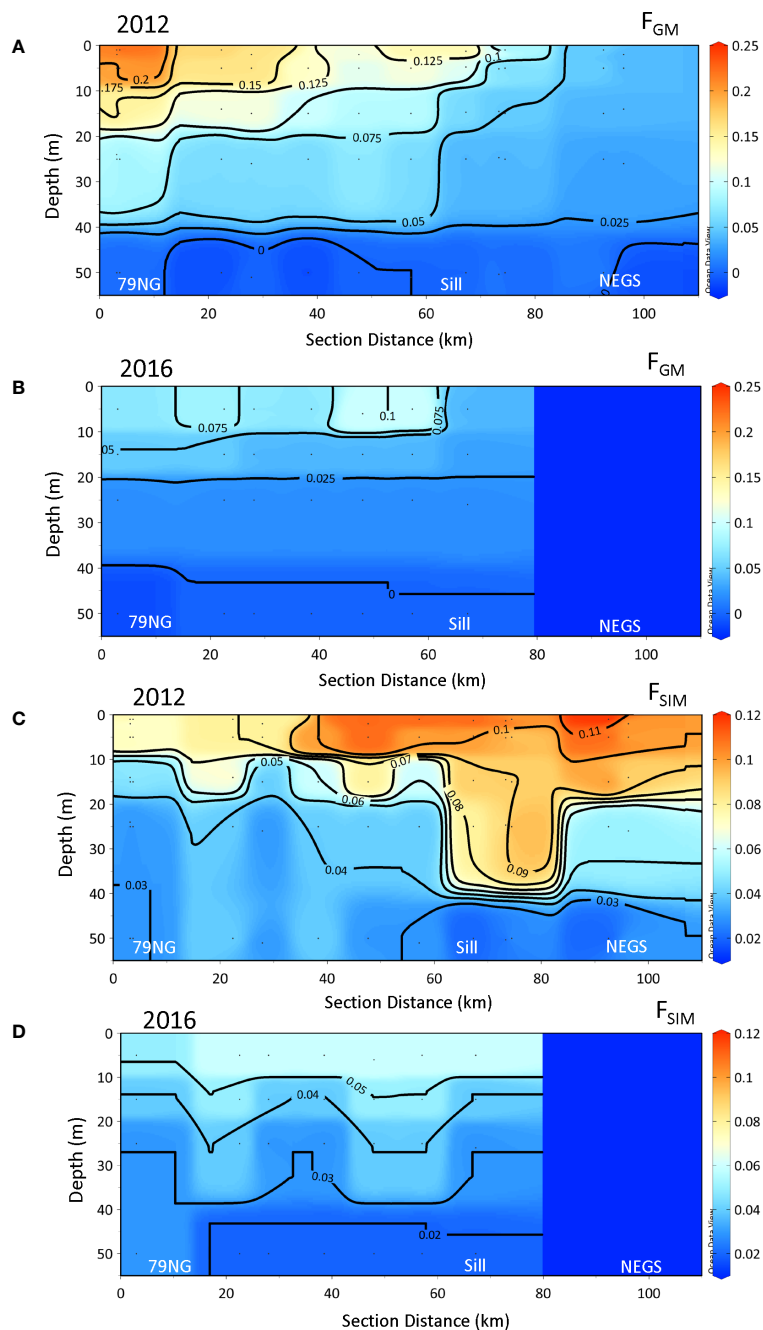


FIGURE 5

The distribution of glacial meltwater fractions ( $F_{GM}$ ) and sea-ice meltwater fractions ( $F_{SIM}$ ) in 2012 (A, C) and in 2016 (B, D) from the 79NG front (distance 0 km) in Dijnphna Sound (DS) to the Northeast Greenland shelf (NEGS). The dark-blue area on the NEGS in 2016 indicates no data.

that the CHL contained water with a deficit of  $[\text{NO}_3^-]$  relative to  $[\text{PO}_4^{3-}]$  as a result of denitrification.

### 4.3 Effects of drivers

#### 4.3.1 Freshening and primary production

The  $\Omega_{ArFW}$  (decreasing  $\Omega_{Ar}$ ) and  $\Omega_{ArBIO}$  (increasing  $\Omega_{Ar}$ ) had almost counteracting effects on  $\Omega_{ArMEAS}$  with increased  $\text{FW}_{TOT}$  (Equation 2; Figures 7A, B). It is clear that both  $\Omega_{ArFW}$  and  $\Omega_{ArBIO}$

had a large impact counteracting each other (Figures 7A, B).  $\Omega_{ArFW}$  had a larger impact on  $\Omega_{ArMEAS}$  than  $\Omega_{ArBIO}$  in both years, and most evident in 2016. In 2012, most of the  $\Omega_{ArFW}$  was compensated by  $\Omega_{ArBIO}$ , whereas in 2016,  $\Omega_{ArFW}$  dominated. There were clear differences between the 2 years in  $\Delta\Omega_{ArFW}$ , in both magnitude and the distribution in the water column along the section (Figures 8A, B). The largest decrease (negative) of approximately 0.4 in  $\Omega_{Ar}$  caused by freshening was observed in 2012 in the SL near the 79NG front (Figure 8A). However, unexpectedly, this was where the highest  $\Omega_{ArMEAS}$  was observed (Figure 4I), concurrently with the largest  $\Delta\Omega_{ArFW}$ ,

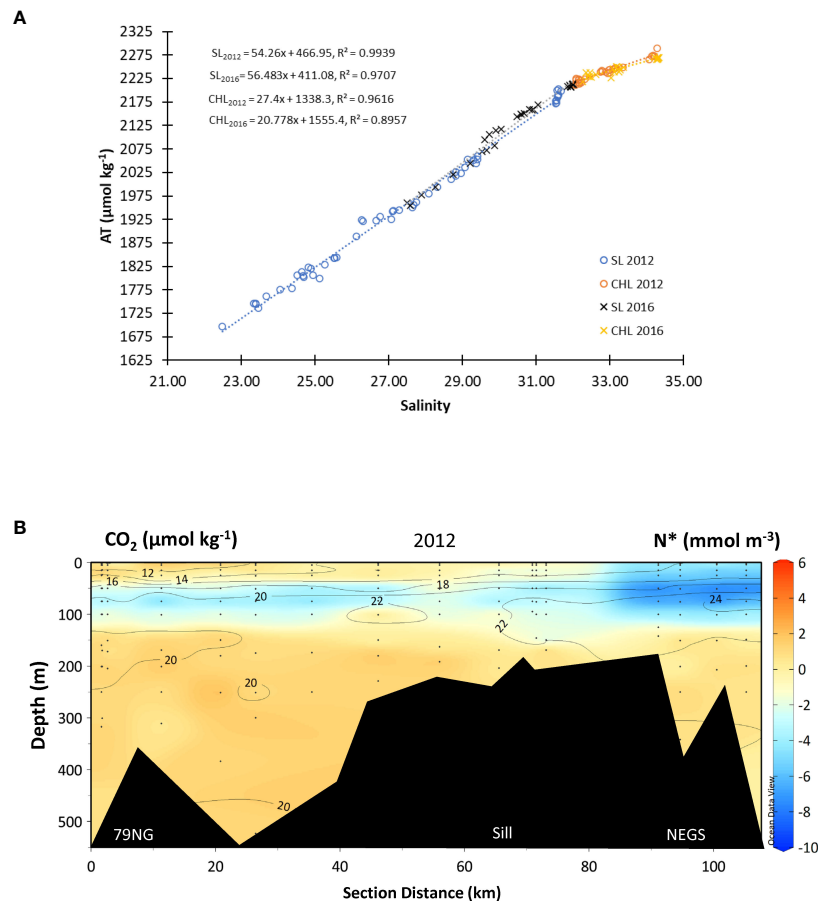


FIGURE 6

Linear relationships between (A) total alkalinity (AT,  $\mu mol\ kg^{-1}$ ) and practical salinity to derive AT in freshwater end members ( $AT_{FWEM}$ , intercept at y-axis) in two layers for the 2 years; surface layer (SL < 50 m, in 2012, blue open circles,  $AT_{SL2012} = 54.289xS + 467, R^2 = 0.99, n = 55$ ), in 2016, black cross,  $AT_{SL2016} = 46.48xS + 411.08, R^2 = 0.97, n = 29$ ; in cold halocline layer (CHL) (2012, orange open circles,  $AT_{CHL2012} = 27.4xS + 1338, R^2 = 0.96, n = 29$ ), in 2016, yellow cross,  $AT_{CHL2016} = 20.78xS + 1555, R^2 = 0.90, n = 24$ ).  $R^2$  denotes the coefficient of determination. Linear relationship on the NEGS (not shown in figure) as follows:  $AT_{SL2012} = 59.885xS + 299.31, R^2 = 0.977$ ;  $AT_{SL2016} = 59.646xS + 330.32, R^2 = 0.9766$ ;  $AT_{CHL2012} = 26.043xS + 1376.3, R^2 = 0.9151$ ;  $AT_{CHL2016} = 16.875xS + 1696.7, R^2 = 0.9452$ . The variability (B) of the semiconservative tracer  $N^*$  (color bar,  $mmol\ m^{-3}$ ) overlaid with values and contours of carbon dioxide concentration ( $CO_2, \mu mol\ kg^{-1}$ ) from the 79NG front to the NEGS in 2012.

indicating that  $\Delta\Omega_{ArBIO}$  compensated the negative effects of  $\Delta\Omega_{ArFW}$ , as observed also in Figure 7A. In 2012, the  $\Delta\Omega_{ArFW}$  effect was three times higher than in 2016 where SL was less stratified than was observed in 2012 (Figure 8B). In 2012, the largest  $\Omega_{Ar}$  increase due to  $\Delta\Omega_{ArBIO}$  of up to 0.6 was, similar to  $\Delta\Omega_{ArFW}$ , found at the 79NG front (Figure 8C). In 2016, high  $\Delta\Omega_{ArBIO}$  values of 0.5 and 0.3 were only found at two stations around 20 km and 60 km from the 79NG front, respectively (Figure 8D). On the NEGS, the increase in  $\Omega_{ArMEAS}$  by  $\Delta\Omega_{ArBIO}$  was at most 0.3 in 2012 and 0.1 in 2016 (Figure 8D).

#### 4.3.2 Air-sea exchange and calcium carbonate dissolution

The integrated  $\Delta AT_{DIFF}$  and  $\Delta DIC_{DIFF}$  (Equation 11) were generally positive (gain) in both years (Figures 9A, B) and in 2012 twice as large as in 2016. The positive  $\Delta AT_{DIFF}$  and  $\Delta DIC_{DIFF}$  suggested a net addition of AT or DIC. Near the 79NG

front, the  $\Delta AT_{DIFF}$  and  $\Delta AT_{GLAC}$  (Equation 12) were almost of the same magnitude in both 2012 and 2016, suggesting that most of the  $\Delta AT_{DIFF}$  can be explained by glacial water-transported carbonate minerals or sea-ice-derived ikaite (Figures 9A, B). In DS, sill, and on the NEGS,  $\Delta AT_{DIFF}$  and  $\Delta AT_{GLAC}$  clearly differed up to 1.5 mol C  $m^{-2}$ , particularly observed in 2012 (Figure 9A), implying other effects than dissolved carbonate minerals. The  $\Delta DIC_{GLAC}$  explained around half of the  $\Delta DIC_{DIFF}$  at 79NG and in the DS in 2012.

In 2012, the  $\Delta DIC_{REST}$  (Equation 13) was generally positive, with a maximum of 2.5 mol C  $m^{-2}$  suggesting a DIC gain from ocean  $CO_2$  uptake (Figure 9A). In 2016, the  $\Delta DIC_{REST}$  varied between being a loss of DIC (ocean  $CO_2$  source) near the 79NG front and sill and a DIC gain (ocean  $CO_2$  uptake) in the DS (Figure 9B).

The  $[CO_3^{2-}]$  related to salinity (S) in DS were generally 10–20  $\mu mol\ kg^{-1}$  higher in 2012 than those in 2016 (Figure 10A). In 2016,

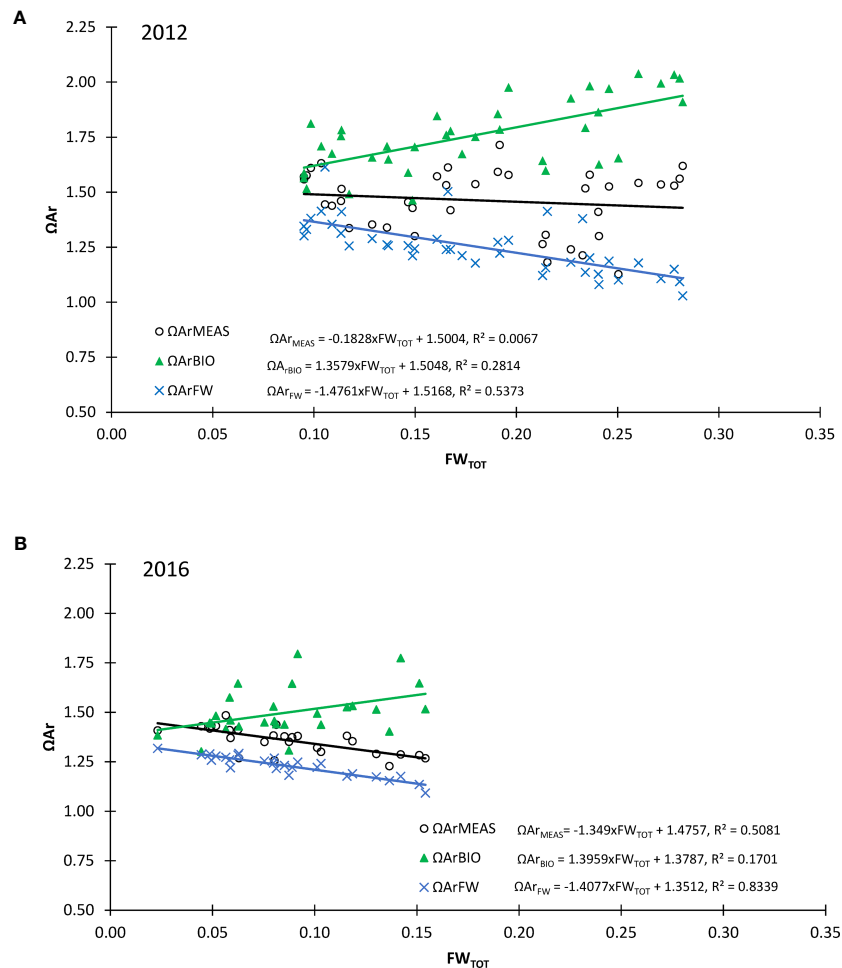


FIGURE 7

Aragonite saturation ( $\Omega_{Ar}$ , y-axis) against total freshwater content ( $FW_{TOT}$ , x-axis) obtained from AT and DIC ( $\Omega_{ArMEAS}$ , black open circles, black regression line), the aragonite saturation due to the freshwater effect ( $\Omega_{ArFW}$ , blue crosses, blue regression line), and the aragonite saturation due to the effect of biological  $CO_2$  drawdown ( $\Omega_{ArBIO}$ , green pyramids, green regression line) for (A) 2012 and (B) 2016. Results of linear regression are shown in the legend and are for 2012: ( $\Omega_{ArBIO} = 1.3579 \times FW_{TOT} + 1.5048, R^2 = 0.2814$ ;  $\Omega_{ArFW} = -1.4761 \times FW_{TOT} + 1.5168, R^2 = 0.5373$ ;  $\Omega_{ArMEAS} = -0.1828 \times FW_{TOT} + 1.5004, R^2 = 0.0067$ ) and for 2016: ( $\Omega_{ArBIO} = 1.3959 \times FW_{TOT} + 1.3787, R^2 = 0.1701$ ;  $\Omega_{ArMEAS} = -1.349 \times FW_{TOT} + 1.4757, R^2 = 0.5081$ ;  $\Omega_{ArFW} = -1.4077 \times FW_{TOT} + 1.3512, R^2 = 0.8339$ ).

the DS values were similar to those on the NEGS (Figure 10A). This suggests that the waters in the DS in 2016 were more influenced by water from the NEGS than in 2012. In 2016, the low AT:S (<70) at high  $\delta^{18}O$  (>-4‰) in the DS indicated more seawater influence (AT:S of 67; Fransson et al., 2020), as was also observed on the NEGS (Figure 10B). In 2012 in DS, the AT:S was up to 75.5 at a  $\delta^{18}O$  of -9‰, confirming carbonate minerals contributing to AT in the meltwater (Figure 10B).

Relations between  $\Delta A_{TDIFF}$  and  $\delta^{18}O$  and between  $\Delta DIC_{DIFF}$  and  $\delta^{18}O$  showed increasing  $\Delta A_{TDIFF}$  and  $\Delta DIC_{DIFF}$  with decreasing  $\delta^{18}O$  (Figures 10C, D). Deviations from the linear relation at  $\Delta A_{TDIFF}$  vs.  $\Delta DIC_{DIFF}$  indicated that processes resulted in both a loss and a gain, such as air-sea  $CO_2$  exchange and  $CaCO_3$  dissolution/precipitation (Figure 10E).  $\Delta A_{TDIFF}$  values above the regression line indicated the contribution of  $[CO_3^{2-}]$ , adding to AT of up to  $70 \mu mol kg^{-1}$  (Figure 10E).  $\Delta DIC_{DIFF}$  values below the regression line indicated ocean  $CO_2$  uptake (increasing DIC but not AT) from the atmosphere up to  $50 \mu mol kg^{-1}$  (Figure 10E).

## 5 Discussion

### 5.1 Comparison with other Arctic fjords and shelves

Spitsbergen and southern Greenland fjords are experiencing changes in ocean chemistry due to freshening from glacial meltwater and sea-ice melt (e.g., Fransson et al., 2015; Fransson et al., 2016; Ericson et al., 2019a; Cantoni et al., 2020; Fransson et al., 2020; Henson et al., 2022), which results in lower  $\Omega_{Ar}$  (e.g., Chierici and Fransson, 2009; Azetsu-Scott et al., 2010; Sejr et al., 2011; Azetsu-Scott et al., 2014) and threatens the productivity and biodiversity in these fjords. In our study, both glacial water and sea-ice melt in SL resulted in decreased  $\Omega_{Ar}$ ,  $pH_T$ , and decreased buffering capacity in both years. The DS was affected by a marine-terminating glacier, with particularly large  $F_{GM}$  observed in the SL near the 79NG front in 2012. This could be caused by the reported extreme melt that occurred on the GrIS in 2012 (Nghiem et al.,

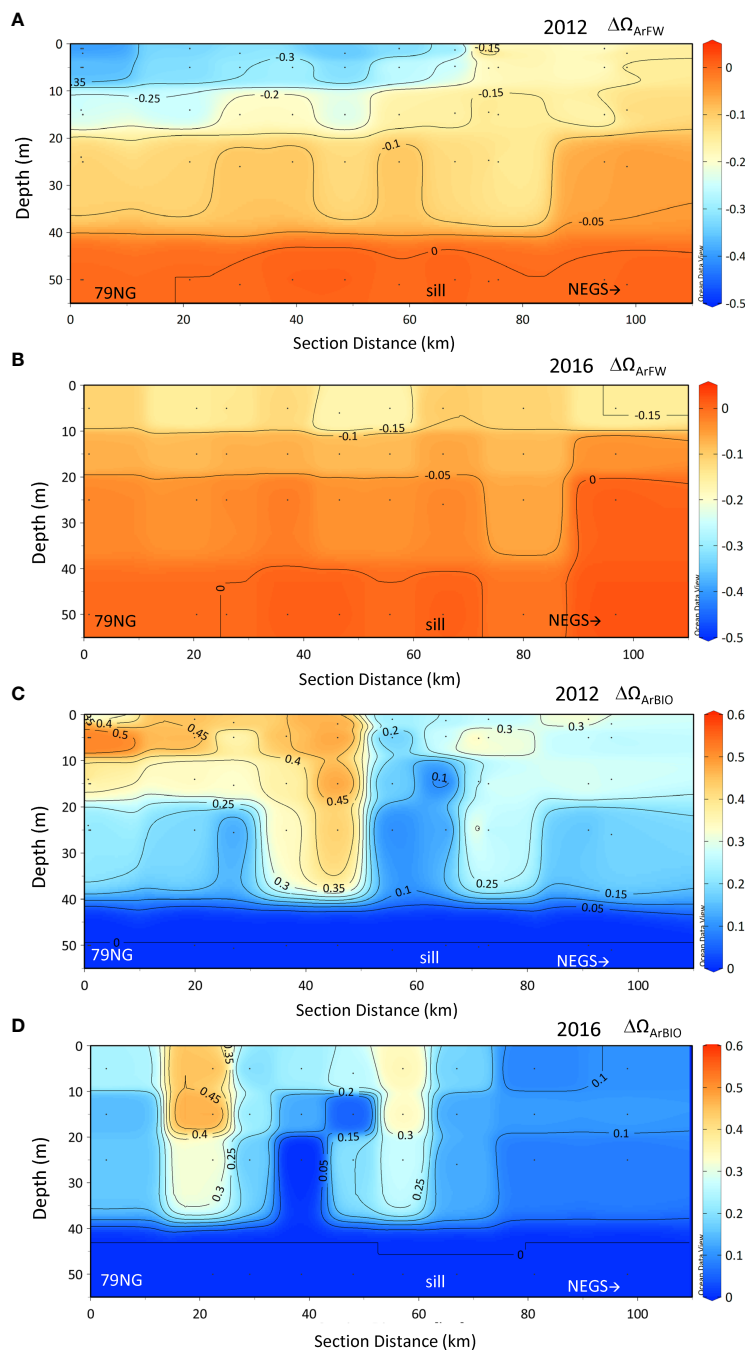


FIGURE 8

Change in  $\Delta\Omega_{Ar}$  due to freshwater ( $\Delta\Omega_{ArFW}$ ) and biological  $\text{CO}_2$  drawdown ( $\Delta\Omega_{ArBIO}$ ) in 2012 (A, C) and in 2016 (B, D) in the upper 50 m. Positive values denote  $\Omega_{Ar}$  increase and negative values indicate a decrease in  $\Omega_{Ar}$  compared with the reference water  $\Omega_{ArREF}$ .

2012). On the NEGS and in DS in 2016, the freshwater in the SL was mostly derived from sea-ice melt.

In our study,  $\Omega_{Ar}$  in the SL in DS was oversaturated ( $\Omega_{Ar} > 1$ ) and varied between 1.13 and 1.63 in 2012 and between 1.27 and 1.43 in 2016 (Table S2). Henson et al. (2022) found large  $\Omega_{Ar}$  variability including corrosive conditions in the surface at times in both the eastern side ( $\Omega_{Ar}$  0.7–3.1) and western ( $\Omega_{Ar}$  0.3–3.1) side of Greenland. In the high-latitude Cumberland Sound, Canada, Turk et al. (2016) reported  $\Omega_{Ar}$  ranging from 1.9 in the surface to 1.4 in the subsurface waters. In Kongsfjorden,  $\Omega_{Ar}$  was always  $> 1$ , with the

lowest  $\Omega_{Ar}$  in the inner part of the fjord due to glacial meltwater (Fransson et al., 2016; Cantoni et al., 2020). The combined effect of freshwater dilution and atmospheric  $\text{CO}_2$  absorption in Kongsfjorden decreased  $\Omega_{Ar}$  to values down to 1.07 that negatively can affect marine calcifiers (Cantoni et al., 2020). We observed the lowest AT in the warmest and freshest water in 2012, as a signal of surface warming and dilution by glacial meltwater. In 2012, the largest glacial meltwater (79NG front, Figure 5A) resulted in the largest increase in  $\Delta\Omega_{ArBIO}$  and highest  $\Omega_{ArMEAS}$  and  $\text{pH}_T$  as well as the largest decrease in  $\Delta\Omega_{ArFW}$  (Figure 8). We found that PP

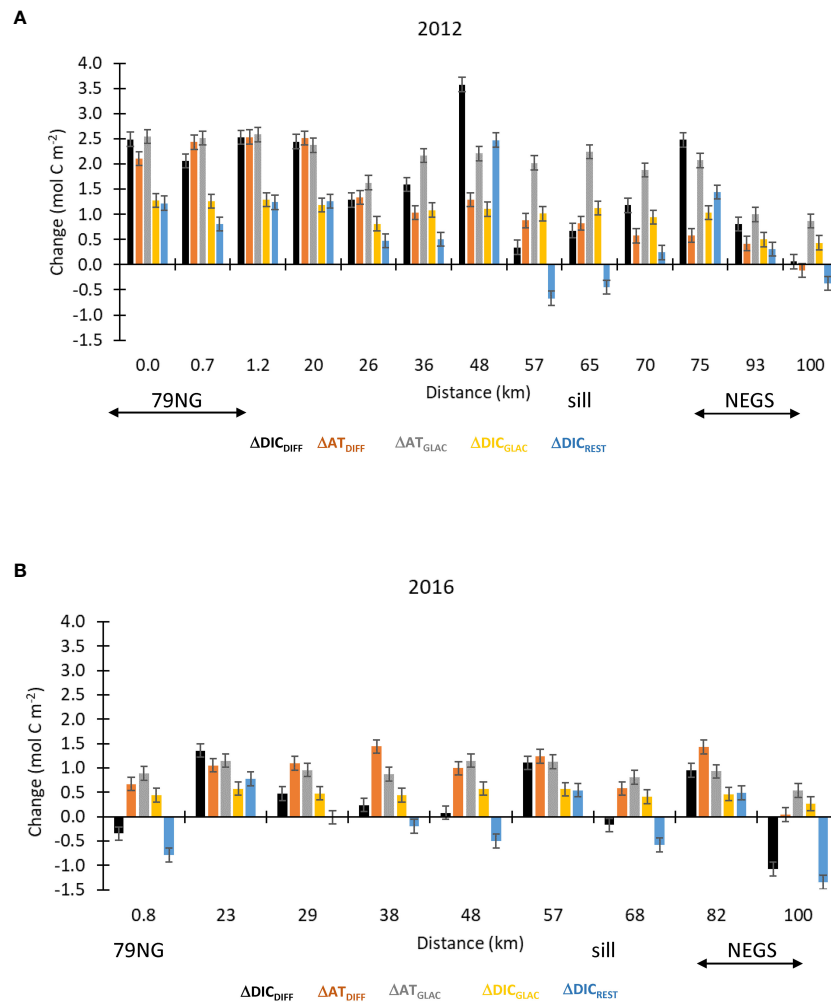


FIGURE 9

The integrated (trapezoidal) change in AT and DIC ( $\text{mol C m}^{-2}$ ) in the surface layer (SL) from the 79NG front to the Northeast Greenland shelf (NEGS) shown as  $\Delta\text{DIC}_{\text{DIFF}}$  (black),  $\Delta\text{AT}_{\text{DIFF}}$  (orange),  $\Delta\text{AT}_{\text{GLAC}}$  (gray),  $\Delta\text{DIC}_{\text{GLAC}}$  (yellow), and  $\text{DIC}_{\text{REST}}$  (blue) in (A) 2012 and (B) in 2016. Positive values denote a gain and negative values denotes a loss of AT or DIC. The error bars indicate the uncertainty based on cumulative error from the analytical precision in the measured parameters ( $\pm 0.14 \text{ mol C m}^{-2}$ ).

compensated for decreased  $\Omega_{\text{Ar}}$  by 0.6–0.9 due to freshwater dilution. This implied that meltwater resulted in beneficial conditions for PP in the SL, perhaps due to stratification resulting in increased availability of inorganic nutrients. This is similar to the stratification meltwater-induced spring blooms observed at the sea-ice edge on the Arctic shelves (e.g., Chierici et al., 2019). This contrasted with the situation in 2016 when DS was less stratified and well mixed with water derived from the NEGS where  $\Delta\Omega_{\text{ArBIO}}$  did not fully compensate for the freshwater dilution by sea-ice meltwater ( $F_{\text{SIM}}$ ). Impacts on  $\Omega_{\text{Ar}}$  due to freshwater and compensations due to biological  $\text{CO}_2$  drawdown were also reported in several West Spitsbergen (Svalbard) fjords; in Kongsfjorden, Fransson et al. (2016) found that glacial water in the inner part of Kongsfjorden decreased  $\Omega_{\text{Ar}}$  by 0.7 and that PP compensated for freshwater dilution effects. Ericson et al. (2019a) found that PP resulted in the largest  $\Omega_{\text{Ar}}$  increase of 0.9, observed in Tempelfjorden in June–August 2015–2017, which compensated for the decrease in  $\Omega_{\text{Ar}}$  due to freshening from dilution of ions due to

glacial meltwater. In other Greenland fjords and West Spitsbergen fjords, similar observations were made. Henson et al. (2022) found that  $\Omega_{\text{Ar}}$  was mainly controlled by PP on the western side of Greenland whereas meltwater dilution of AT controlled the eastern side of Greenland. In the Godthåbfjorden (Greenland), Meire et al. (2015) found that the decreasing effects of AT dilution may be compensated by photosynthesis in productive Greenland fjords. However, in the absence of significant biological activity, diluted AT may lead to reduced  $\Omega_{\text{Ar}}$  and corrosive conditions.

On the West Spitsbergen shelf, calcium carbonate dissolution contributed to a DIC increase of between 0.1 and 0.55  $\text{mol C m}^{-2}$  in the upper 50 m from January to August based on a similar method as here (Chierici et al., 2019). This is similar to the  $\Delta\text{DIC}_{\text{GLAC}}$  values in the NEGS (both years) and in DS in 2016, and around half the size as the  $\Delta\text{DIC}_{\text{GLAC}}$  at the 79NG front and DS in 2012 (Figure 9A). One explanation to the twice as high contribution of carbonate minerals in 2012 at the 79NG front and in DS is the relatively larger influence of glacial meltwater, which plays a minor

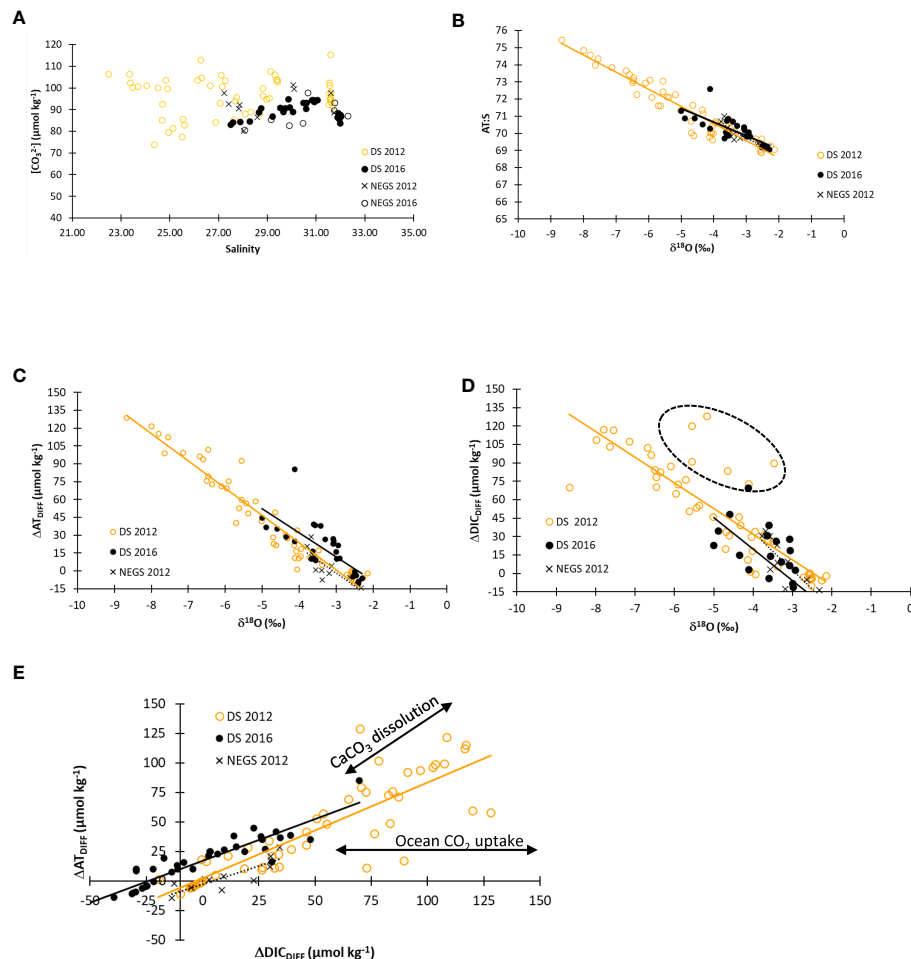


FIGURE 10

(A) Carbonate ion concentration ( $[\text{CO}_3^{2-}]$ ,  $\mu\text{mol kg}^{-1}$ ) versus practical salinity for Dismal Sound (DS) in 2012 (DS 2012, yellow open circles) and in 2016 (DS 2016, closed black circles), and on the Northeast Greenland shelf (NEGS) in 2012 (NEGS 2012, black cross) and in 2016 (NEGS 2016, black open circles). (B) Salinity and total alkalinity ratio (AT:S, y-axis) versus  $\delta^{18}\text{O}$  (‰, x-axis). (C)  $\Delta\text{AT}_{\text{DIFF}}$  ( $\mu\text{mol kg}^{-1}$ ) versus  $\delta^{18}\text{O}$  (‰, x-axis). (D)  $\Delta\text{DIC}_{\text{DIFF}}$  ( $\mu\text{mol kg}^{-1}$ ) versus  $\delta^{18}\text{O}$  (‰, x-axis). (E)  $\Delta\text{AT}_{\text{DIFF}}$  ( $\mu\text{mol kg}^{-1}$ , y-axis) versus  $\Delta\text{DIC}_{\text{DIFF}}$  ( $\mu\text{mol kg}^{-1}$ , x-axis). The dashed ovals in (D) show data points deviating from the regression line. For symbol references see (A). Figures (B–D) show regression lines to indicate deviations and refer to the following, DS 2012 (yellow); DS 2016 (black); and NEGS 2012 (black dashed). Black arrows in (E) denote the effect of calcium carbonate ( $\text{CaCO}_3$ ) dissolution and air-sea  $\text{CO}_2$  exchange on  $\Delta\text{AT}_{\text{DIFF}}$  and  $\Delta\text{DIC}_{\text{DIFF}}$ .

role on the West Spitsbergen shelf and NEGS. Chierici et al. (2019) explained that most of the  $\text{CaCO}_3$  contribution was from advected  $\text{CaCO}_3$  shells and from sea-ice meltwater ikaite dissolution.

The  $\Delta\text{AT}_{\text{GLAC}}$  varied between  $2.6 \text{ mol C m}^{-2}$  at the 79NG front and  $0.9 \text{ mol C m}^{-2}$  on the NEGS (Figure 9A) in our study. Correspondingly in 2016, the  $\Delta\text{AT}_{\text{GLAC}}$  varied between  $0.5 \text{ mol C m}^{-2}$  (NEGS) and  $1.2 \text{ mol C m}^{-2}$  in the DS (Figure 9B). In 2012 in DS, the relation between AT:S and  $\delta^{18}\text{O}$  showed that  $\delta^{18}\text{O}$  values lower than  $-2\text{‰}$  ( $-3$  to  $-9\text{‰}$ ) corresponded to AT:S between 70 and 75.5 (Figure 10B), which has also been observed in Tempelfjorden near the glacier front (Fransson et al., 2015; Fransson et al., 2020).

$\text{AT}_{\text{FWEM}}$  in SL on the NEGS was ( $299$ – $336 \mu\text{mol kg}^{-1}$ ), which was lower than in DS ( $411$ – $467 \mu\text{mol kg}^{-1}$ ). Sea-ice meltwater in our study area had an AT value of around  $150 \mu\text{mol kg}^{-1}$ , measured in melted sea ice in western Fram Strait (Fransson and Chierici, 2023). This could potentially be another source of buffering ions as observed in West Spitsbergen fjords such as Tempelfjorden

(Fransson et al., 2015; Fransson et al., 2020) and on the West Spitsbergen shelf (Chierici et al., 2019).

The Arctic rivers contribute substantially to AT in CHL with reported AT values of Arctic rivers varying between  $1,000$  and  $1,500 \mu\text{mol kg}^{-1}$  (e.g., Cooper et al., 2008; Fransson et al., 2001). This is within the range of  $\text{AT}_{\text{FWEM}}$  estimated in the CHL waters of DS and NEGS of around  $1,340$ – $1,555 \mu\text{mol kg}^{-1}$  and  $1,360$ – $1,690 \mu\text{mol kg}^{-1}$ , respectively. This agrees well with the fact that Arctic rivers are a major freshwater source in the CHL, as evident from other tracers such as DOM (Stedmon et al., 2015) and the most negative  $\text{N}^*$  ( $-10 \mu\text{mol L}^{-1}$ ; Figure 5B; Equation 14) and the highest  $\text{CO}_2$  concentration ( $>24 \mu\text{mol kg}^{-1}$ ) (Figure 5B), from mineralized organic carbon in the CHL (Figure 5B). This is consistent with the findings by Anderson et al. (2013), which further support the origin of CHL from the Arctic shelves.

$\Delta\text{DIC}_{\text{REST}}$  (Equation 13) indicated the contribution of air-sea  $\text{CO}_2$  exchange to the DIC change, where the positive values in large parts in DS in 2012 denoted a gain in DIC due to ocean  $\text{CO}_2$  uptake

(Figure 9A). In 2012, the  $\Delta\text{DIC}_{\text{REST}}$  was maximum  $2.5 \text{ mol C m}^{-2}$  (Figure 9A). Chierici et al. (2019) found that the ocean acted as a  $\text{CO}_2$  sink of up to  $2.1 \text{ mol C m}^{-2}$  with an average of  $1 \text{ mol C m}^{-2}$  on the West Spitsbergen shelf in August. However, by the end of August, the ocean showed a  $\text{CO}_2$  loss to the atmosphere of around  $0.7 \text{ mol C m}^{-2}$  (Chierici et al., 2019). In our study, we find a loss of up to  $1.5 \text{ mol C m}^{-2}$  on the NEGS in 2016 (Figure 9B). In Tempelfjorden, there was estimated an ocean  $\text{CO}_2$  sink of  $0.8 \text{ mol C m}^{-2}$  in the upper 20 m (Fransson et al., 2015).

Both years had surface  $f\text{CO}_2$  values that were lower than the atmospheric  $\text{CO}_2$  level of  $415 \mu\text{atm}$  (Ny-Ålesund, Zeppelin Mountain), most pronounced in 2012 where  $f\text{CO}_2$  was as low as around  $140 \mu\text{atm}$  at the 79NG front and around  $250 \mu\text{atm}$  on the NEGS (Figure 4E). In 2016,  $f\text{CO}_2$  was around  $275\text{--}300 \mu\text{atm}$  throughout the section (Figure 4F). Undersaturated surface  $f\text{CO}_2$  was caused by both PP and meltwater and resulted in a capacity to take up atmospheric  $\text{CO}_2$ , particularly in 2012. Meire et al. (2015) also found surface  $f\text{CO}_2$  (i.e.,  $p\text{CO}_2$  in their study) values in August between  $100 \mu\text{atm}$  and  $120 \mu\text{atm}$  at the inner fjord near the GrIS, which is similar to our values in 2012 at 79NG front. Meire et al. (2015) explained the low  $f\text{CO}_2$  caused by high glacial meltwater input and PP during the summer months. In Tempelfjorden (W. Spitsbergen), the lowest surface  $f\text{CO}_2$  was  $140 \mu\text{atm}$  in summer (Ericson et al., 2019a), similar to our study in 2012. In Young Sound, NE Greenland, an annual ocean  $\text{CO}_2$  uptake of  $2.7 \text{ mol CO}_2 \text{ m}^{-2} \text{ yr}^{-1}$  was estimated by Sejr et al. (2011), which was similar to the estimated  $\text{CO}_2$  uptake in Adventfjorden, West Spitsbergen, by Ericson et al. (2019b). These studies were based on seasonal *in situ*  $f\text{CO}_2$  observations and thus a different time scale than in our method. We used an integrated approach of drivers in the upper 50 m based on concentrations in a reference water; hence, it is difficult for direct comparison of the results. However, using our data ( $f\text{CO}_2$ , S, T) in the surface water (upper 15 m), the atmospheric level of  $415 \mu\text{atm}$ , and the mean August wind speed of  $7 \text{ m s}^{-1}$  by Wanninkhof (2014) flux formulation, we obtained a mean monthly ocean  $\text{CO}_2$  sink of  $0.9 \pm 0.2 \text{ mol C m}^{-2}$  in 2012 and  $0.6 \pm 0.1 \text{ mol C m}^{-2}$  in 2016. Assuming 3 months of open water for air-sea exchange, this means  $2.7$  and  $1.8 \text{ mol C m}^{-2}$  for 2012 and 2016, respectively. Similar estimates were conducted for Tempelfjorden, where the ocean  $\text{CO}_2$  sink corresponded to  $0.11 \text{ mol m}^{-2} \text{ month}^{-1}$  and  $0.8 \text{ mol C m}^{-2}$  for the open water period (Fransson et al., 2015). This calculation shows the potential for our area to act as a  $\text{CO}_2$  sink caused by both freshening and PP.

## 5.2 Uncertainty

Contribution of organic acids to AT in coastal areas, fjords, and estuaries usually results in high AT at low salinities (Liang et al., 2020). Organic acids are mainly found in waters with high dissolved organic matter. To have a significant influence on AT, the concentrations of acids must be  $>10 \mu\text{mol kg}^{-1}$ , and this has been observed in bays with restricted seawater exchange and large

anthropogenic influence (e.g., Liang et al., 2020) and in culture studies and highly productive coastal sites with high inorganic  $[\text{NO}_3^-]$  ( $70 \text{ mol kg}^{-1}$ ; Ko et al., 2016) and dissolved organic carbon (DOC; up to 10 times seawater concentrations). In our study, there was little organic matter supplied by local runoff (Stedmon et al., 2015) and low-turbidity surface water (Granskog et al., in review) and we could not observe any clear deviations based on the AT-S relationship (Figure 6A). Moreover, the largest deviation from  $\Delta\text{AT}\text{--}\Delta\text{DIC}$  relationship was observed in the  $\Delta\text{DIC}$  and not in the  $\Delta\text{AT}$  values (Figures 10C, D). This implies that there is no clear evidence of organic acids/bases that can influence AT values to a significant degree. Other studies from Greenland show that the DOC concentrations in the glacial runoff from the GrIS were low and at most  $15 \mu\text{mol L}^{-1}$  ( $<1 \text{ mg L}^{-1}$ ) and the DOC originated from river runoff (Paulsen et al., 2017). In the DS and NEGS, there are no river runoff; thus, the DOC concentration was likely too low to have any significant effects on AT in our study.

Carbonate minerals in the SL water samples, derived from the bedrock (e.g., calcite, dolomite) or sea ice (e.g., ikaite), can be dissolved during analyses. This can give an increase in AT relative to S, and we investigated the deviation (excess AT) in the AT-S relationship (Figure 10E). On a few occasions in our study, we observed deviation in AT from S coinciding with a positive  $\text{AT}_{\text{GLAC}}$  (Figure 9) particularly evident near the 79NG front, which is considered in our approach.

The effect of different C:P ratios on  $\Delta\text{DIC}_{\text{BIO}}$  is directly proportional to the change in the ratio. Studies have shown large C:P variability connected to temporal and spatial variability, physical and chemical processes, and the stage and type of bloom (Anderson and Sarmiento, 1994; Tanioka et al., 2022). There are few estimates of C:P ratios on the Arctic shelves and fjords partly because most of the estimates on  $\text{DIC}_{\text{BIO}}$  use C:N ratio (Chierici et al., 2011; Frigstad et al., 2014; Jones et al., 2020). Frigstad et al. (2014) showed that the C:N ratio ranged from 6.4 to 8.8 due to regional differences. Since the change is proportional to the change in the ratio (Treguer et al., 1990), this would cause a change in  $\text{DIC}_{\text{BIO}}$  between 3% and 25%. This agrees with the relative change to  $\text{DIC}_{\text{BIO}}$  caused by the reported C:P variability of  $\pm 14$  (Anderson and Sarmiento, 1994) and  $\pm 25$  (Tanioka et al., 2022), which translates to a 13% to 24% change in  $\text{DIC}_{\text{BIO}}$ .

## 5.3 Future perspective and climate change

Ongoing warming and increased meltwater due to climate change will impact drivers and OA. Recently, melting of glacial ice has been reported due to the increasing presence and warming of Atlantic water (Atlantification) by marine-terminating glaciers in northeast Greenland fjords (Straneo et al., 2010; de Steur et al., 2014; Gjelstrup et al., 2022), which will further accelerate glacier melt in the GrIS. In June 2020, the Spalte Gletcher drastically split off from the 79NG and has essentially disappeared (<https://eng.geus.dk/about/news/news-archive/2020/september/glacier>), which in

future can have implications for the hydrography and biogeochemistry in the DS. Moreover, recent findings report on a shoaling of AW (de Steur et al., 2023), so Atlantification may play a greater role in the future. Melting of sea ice on the NEGS could also increase due to the intrusion of warmer AW. Less sea ice will create both more freshwater and more open water for potentially higher CO<sub>2</sub> uptake by the ocean. In a scenario of (1) increased freshwater leading to stronger surface water stratification, such as the situation in 2012, PP will be stimulated in a more stratified SL. Interestingly, in our study near the sill,  $\Delta\text{DIC}_{\text{REST}}$  changed from the largest positive value (CO<sub>2</sub> uptake from atmosphere) to a negative value (ocean CO<sub>2</sub> source) in both years (Figure 9). This was also the same location where  $\Delta\Omega_{\text{ArBIO}}$  changed from high to low values in 2012 (Figure 8C), which can be an effect of decreased stratification in SL resulting in lower  $\Delta\Omega_{\text{ArBIO}}$ . However, at some point, stratification may limit the renewal of inorganic nutrients resulting in less compensatory effect in  $\Omega_{\text{Ar}}$  by PP. Another scenario of (2) subglacial melting due to Atlantification will cause upwelling and bring nutrient-rich water to the surface that will stimulate PP and compensate and increase  $\Omega_{\text{Ar}}$ . On the other hand, AW is also rich in DIC as well as AT, which can promote further ocean CO<sub>2</sub> uptake.

Another possibility, similar to the situation in 2016, is when NEGS water was prominent in DS with relatively low  $\Omega_{\text{Ar}}$  (<1.4) in SL and down to <1.2 in the CHL. Since this water was mixed in the water column, calcifying organisms have less possibility to escape unfavorable  $\Omega_{\text{Ar}}$  conditions, as was discussed in Fransson et al. (2016). Moreover, autumn mixing also brings high CO<sub>2</sub> and low  $\Omega_{\text{Ar}}$  subsurface CHL waters to the surface as found in the Canadian Arctic Archipelago (Chierici et al., 2011). This is also a critical time for juveniles of some species of calcifying organisms, such as shelled butterfly snails (*Limacina helicina*). Projections of the change of OA state by increased meltwater showed that by accounting only for the effect of freshening, the projected undersaturation level ( $\Omega_{\text{Ar}<1}$ ) was found at  $\text{FW}_{\text{TOT}}$  of 0.35 and corrosive  $\Omega_{\text{Ar}}$  conditions would have been the case without the counteracting biological effect (Figure 7).

Increased glacial melt of the GrIS was measured as the increased net ablation of 2.2 m + 17% (anomaly) between January and August 2022 measured at Kronprins Christian Land station on northeast Greenland (Moon et al., 2022). The net ablation was even larger in the southeast Greenland, of 4.3 m + 21% (anomaly, at Tasiliq), indicating increased GrIS runoff. Assuming increased net ablation of the GrIS in the northeast Greenland as in the southern Greenland, surface freshening with increasingly corrosive conditions would occur earlier, as was found in the Greenland fjords by Henson et al. (2022). In 2012, an extremely high loss of GrIS due to surface melt was discovered by Nghiem et al. (2012). With the future warming and increased meltwater, our results on the higher  $F_{\text{GM}}$  in 2012 than in 2016 and effects on  $\Omega_{\text{Ar}}$  can possibly be indicative of future conditions under continued warming.

## 6 Conclusion

In this study, we found that the combined effects of glacial and sea-ice meltwater dilution resulted in enhanced ocean acidification in the Dijnphna Sound and Northeast Greenland shelf. However, in summer low aragonite saturation state was compensated by biological CO<sub>2</sub> drawdown, most evident at the 79NG front in 2012. This was potentially caused by meltwater-induced surface stratification leading to favorable conditions for phytoplankton blooms. Surface waters were undersaturated in  $f\text{CO}_2$  relative to the atmospheric  $f\text{CO}_2$  level with relatively large undersaturation near the 79NG calving front, suggesting a large potential for uptake of atmospheric CO<sub>2</sub> during the ice-free season. The low  $f\text{CO}_2$  was mainly a result of a combination of biological CO<sub>2</sub> uptake and dilution due to freshwater. However, so far, there is limited knowledge about seasonal and interannual variability of the drivers and the effects on the ocean acidification in North Greenland fjords. Another observational challenge is the different characteristics in sill depth, bedrock composition, sea-ice cover, and biogeochemistry of fjords and coastal systems.

In a future climate of warming and freshening from increased supply of glacial meltwater and subglacial meltwater, the negative effect (lowering  $\Omega_{\text{Ar}}$ ) on  $\Omega_{\text{Ar}}$  may surpass the positive effect (increases  $\Omega_{\text{Ar}}$ ) due to primary production causing a net  $\Omega_{\text{Ar}}$  decrease. Apart from biological processes and freshening, other processes such as physical upwelling of CO<sub>2</sub>-rich subsurface waters also decrease  $\Omega_{\text{Ar}}$ . These processes will become affected in a case of warming, increased freshwater addition, and changes in sea-ice cover and extent, which will all impose feedbacks on ocean acidification.

Changes in carbonate chemistry toward more corrosive  $\Omega_{\text{Ar}}$  conditions have been observed in the Arctic Ocean and on the ice shelves, related to the loss of sea ice and increased ocean CO<sub>2</sub> uptake (Qi et al., 2022). Polar water is transported southward downstream along the East Greenland coast, which could also affect the carbonate system, ocean acidification status, and CO<sub>2</sub> uptake in other Greenland fjords and on the shelf. Greenland (Arctic) fjords are already facing dramatic changes from global warming, such as increased runoff from glacier melt. To assess the net impact of ongoing ocean acidification in the climate-sensitive Arctic shelves and fjords, it is necessary to understand the complex interplay of these processes in a changing climate.

## Data availability statement

The raw data supporting the conclusions of this article will be made available by the authors upon request.

## Author contributions

AF: Conceptualization, Investigation, Formal analysis, Funding acquisition Data curation, Writing – original draft review and editing. MC: Conceptualization, Investigation, Formal analysis, Funding acquisition Data curation, Writing – original draft review and editing. MG: Investigation, – review and editing. PD: Investigation, Data curation. CS: Investigation, Data curation, -review and editing. All authors contributed to the article and approved the submitted version.

## Funding

This work was supported by the Fram Centre Ocean Acidification Flagship at the FRAM - High North Research Centre for Climate and the Environment, and the European Union's Horizon 2020 research and innovation program under grant agreement no. 820989 (project COMFORT), the Ministry of Climate and Environment, and the Ministry of Trade, Industry and Fisheries, Norway.

## Acknowledgments

We are grateful for the support onboard the *R/V Lance* with Captain and crew for technical and logistic support during the two expeditions. We also thank the Norwegian Polar Institute logistics in Longyearbyen for logistic support and safety training. We are grateful for the constructive comments from reviewers that greatly

improved the manuscript. Data will be publicly available at Norwegian Polar Data Centre at the time of publication.

## Conflict of interest

The authors declare that the research was conducted in the absence of any commercial or financial relationships that could be construed as a potential conflict of interest.

## Publisher's note

All claims expressed in this article are solely those of the authors and do not necessarily represent those of their affiliated organizations, or those of the publisher, the editors and the reviewers. Any product that may be evaluated in this article, or claim that may be made by its manufacturer, is not guaranteed or endorsed by the publisher.

## Supplementary material

The Supplementary Material for this article can be found online at: <https://www.frontiersin.org/articles/10.3389/fmars.2023.1155126/full#supplementary-material>

### SUPPLEMENTARY FIGURE 1

The  $\Omega_{Ar}$  values (A) and (B) the difference between  $\Omega_{Ar}$  calculated from the carbonic constants K1 and K2 estimated by Dickson and Millero (1987),  $\Omega_{Ar_{MEAS}}$  (blue dots) and the ones derived from Lueker et al. (2000),  $\Omega_{Ar_L}$  (yellow cross) versus temperature (°C). The dashed black line in (B) shows the mean difference (-0.004) between the  $\Omega_{Ar_{MEAS}}$  and the  $\Omega_{Ar_L}$  ( $\Delta\Omega_{Ar_{MD-L}}$ ).

## References

- Anderson, L. A., and Sarmiento, J. L. (1994). Redfield ratios of remineralization determined by nutrient data analysis. *Glob. Biogeochem. Cycles* 8, 65–80. doi: 10.1029/93GB03318
- Anderson, L. G., Andersson, P. S., Björk, G., Jones, E. P., Jutterström, S., and Wahlström, I. (2013). Source and formation of the upper halocline of the Arctic Ocean. *J. Geophys. Res. Oceans* 118, 410–421. doi: 10.1029/2012JC008291
- Apollonio, S. (1973). Glaciers and nutrients in Arctic seas. *Science* 180, 491–493. doi: 10.1126/science.180.4085.491
- Azetsu-Scott, K., Clarke, A., Falkner, K., Hamilton, J., Jones, E. P., Lee, C., et al. (2010). Calcium carbonate saturation states in the waters of the Canadian Arctic Archipelago and the Labrador Sea. *J. Geophys. Res.* 115, C11. doi: 10.1029/2009JC005917
- Azetsu-Scott, K., Starr, M., Mei, Z.-P., and Granskog, M. (2014). Low calcium carbonate saturation state in an Arctic inland sea having large and varying fluvial inputs: The Hudson Bay system. *J. Geophys. Res.* 119 (9), 6210–6220. doi: 10.1002/2014JC009948
- Bednaršek, N., Naish, K. A., Feely, R. A., Hauri, C., Kimoto, K., Hermann, A. J., et al. (2021). Integrated assessment of ocean acidification risks to pteropods in the northern high latitudes: regional comparison of exposure, sensitivity and adaptive capacity. *Front. Mar. Sci.* 8. doi: 10.3389/fmars.2021.671497
- Bhatia, M. P., Kujawinski, E. B., Das, S. B., Breier, C. F., Henderson, P. B., and Charette, M. A. (2013). Greenland meltwater as a significant and potentially bioavailable source of iron to the ocean. *Nat. Geosci.* 6 (4), 274–278. doi: 10.1038/ngeo1746
- Cantoni, C., Hopwood, M. J., Clarke, J. S., Chiggiato, J., Achterberg, E. P., and Cozzi, S. (2020). Glacial drivers of marine biogeochemistry indicate a future shift to more corrosive conditions in an Arctic Fjord. *J. Geophys. Res. Biogeosci.* 125, (11). doi: 10.1029/2020JG005633
- Carlson, D. F., Pasma, J., Jacobsen, M. E., Hansen, M. H., and Thomsen, S. (2019). Retrieval of ice samples using the ice drone. *Front. Earth Sci.* 7. doi: 10.3389/feart.2019.00287
- Chierici, M., and Fransson, A. (2009). Calcium carbonate saturation in the surface water of the Arctic Ocean: undersaturation in freshwater influenced shelves. *Biogeosciences* 6, 2421–2432. doi: 10.5194/bg-6-2421-2009
- Chierici, M., and Fransson, A. (2018). “Arctic chemical oceanography at the edge: focus on carbonate chemistry,” in *At the Edge*. Ed. P. Wassmann (Stamsund, Norway: Orkana forlag), 343, ISBN: .
- Chierici, M., Fransson, A., Lansard, B., Miller, L. A., Mucci, A., Shadwick, E., et al. (2011). Impact of biogeochemical processes and environmental factors on the calcium carbonate saturation state in the Circumpolar Flaw Lead in the Amundsen Gulf, Arctic Ocean. *J. Geophys. Res.* 116, C00G09. doi: 10.1029/2011JC007184
- Chierici, M., Fransson, A., Turner, D., Pakhomov, E. A., and Froneman, P. W. (2004). Variability in pH,  $fCO_2$ , oxygen and flux of  $CO_2$  in the surface water along a transect in the Atlantic sector of the Southern Ocean. *Deep-Sea Res. II* 51, 2773–2787. doi: 10.1016/j.dsr2.2001.03.002
- Chierici, M., Vernet, M., Fransson, A., and Børshheim, Y. (2019). Net community production and carbon exchange from winter to summer in the Atlantic Water inflow to the Arctic Ocean. *Front. Mar. Sci.* 6. doi: 10.3389/fmars.2019.00528
- Cooper, L. W., McClelland, J. W., Holmes, R. M., Raymond, P. A., Gibson, J. J., Guay, C. K., et al. (2008). Flow-weighted values of runoff tracers ( $\delta^{18}O$ , DOC, Ba, alkalinity) from the six largest Arctic rivers. *J. Geophys. Res.* 35. doi: 10.1029/2008GL035007
- Dauphinee, T. M., and Klein, H. P. (1975). A new automated laboratory salinometer. *Sea Technol.* 16, 23–25.
- de Steur, L., Hansen, E., Mauritzen, C., Beszczynska-Möller, A., and Fahrback, E. (2014). Impact of recirculation on the East Greenland Current in Fram Strait: Results

- from moored current meter measurements between 1997 and 2009. *Deep Sea Res. Part I: Oceanogr. Res. Pap.* 92, 26–40. doi: 10.1016/j.dsr.2014.05.018
- de Steur, L., Sumata, H., Divine, D., Granskog, M. A., and Pavlova, O. (2023). Upper ocean warming and sea ice reduction in the East Greenland Current from 2003 to 2019. *Commun. Earth Environ.* 4, 261. doi: 10.1038/s43247-023-00913-3
- Deutsch, C., Gruber, N., Key, R. M., Sarmiento, J. L., and Ganachaud, A. (2001). Denitrification and N<sub>2</sub> fixation in the Pacific Ocean. *Glob. Biogeochem. Cycles* 15, 483–506. doi: 10.1029/2000GB001291
- Dickson, A. G. (1990). Standard potential of the (AgCl(s) + 1/2H<sub>2</sub>(g) = Ag(s) + HCl(aq)) cell and the dissociation constant of bisulfate ion in synthetic sea water from 273.15 to 318.15 K. *J. Chem. Thermodyn.* 22, 113–127. doi: 10.1016/0021-9614(90)90074-Z
- Dickson, A. G., and Millero, F. J. (1987). A comparison of the equilibrium constants for the dissociation of carbonic acid in seawater media. *Deep-Sea Res. I* 34 (10), 1733–1743. doi: 10.1016/0198-0149(87)90021-5
- A. G. Dickson, C. L. Sabine and J. R. Christian (Eds.) (2007). *Guide to Best Practices for Ocean CO<sub>2</sub> Measurements* Vol. 3 (Sidney, BC, Canada: PICES Special Publication). 191 pp.
- Dodd, P. A., Rabe, B., Hansen, E., Falck, E., Mackensen, A., Rohling, E., et al. (2012). The freshwater composition of the Fram Strait outflow derived from a decade of tracer measurements: composition of the Fram Strait outflow. *J. Geophys. Res. Oceans* 117 (C110005). doi: 10.1029/2012JC008011
- Epstein, S., and Mayeda, T. (1953). Variations of <sup>18</sup>O content of waters from natural sources. *Geochim. Cosmochim. Acta* 4, 213–224. doi: 10.1016/0016-7037(53)90051-9
- Ericson, Y., Chierici, M., Falck, E., Fransson, A. I., Jones, E. M., and Kristiansen, S. (2019b). Seasonal dynamics of the marine CO<sub>2</sub> system in Adventfjorden, a West Spitsbergen fjord. *Polar Res.* 38, 3345. doi: 10.33265/polar.v38.3345
- Ericson, Y., Falck, E., Chierici, M., Fransson, A., and Kristiansen, S. (2019a). Marine CO<sub>2</sub> system variability in a high arctic tidewater-glacier fjord system, Tempelfjorden, Svalbard. *Continental Shelf Res.* 181, 1–13. doi: 10.1016/j.csr.2019.04.013
- Fransson, A., and Chierici, M. (2023). *Chemical variables in sea ice in summers 2012 and 2016 in Fram Strait [Data set]* (Norwegian Polar Institute). doi: 10.21334/npolar.2023.a3040349
- Fransson, A., Chierici, M., Anderson, L. G., Bussman, I., Jones, E. P., and Swift, J. H. (2001). The importance of shelf processes for the modification of chemical constituents in the waters of the eastern Arctic Ocean: implication for carbon fluxes. *Cont. Shelf Res.* 21, 225–242. doi: 10.1016/S0278-4343(00)00088-1
- Fransson, A., Chierici, M., Anderson, L. G., and David, R. (2004). Transformation of carbon and oxygen in the surface layer of the eastern Atlantic sector of the Southern Ocean. *Deep-Sea Res. II* 51 (22–24), 2757–2772. doi: 10.1016/j.dsr.2.2001.12.001
- Fransson, A., Chierici, M., and Nojiri, Y. (2009). New insights into the spatial variability of the surface water CO<sub>2</sub> in varying sea ice conditions in the Arctic Ocean. *Cont. Shelf Res.* 29, 1317–1328. doi: 10.1016/j.csr.2009.03.008
- Fransson, A., Chierici, M., Nomura, D., Granskog, M. A., Kristiansen, S., Martma, T., et al. (2015). Effect of glacial drainage water on the CO<sub>2</sub> system and ocean acidification state in an Arctic tidewater-glacier fjord during two contrasting years. *J. Geophys. Res. Oceans* 120. doi: 10.1002/2014JC010320
- Fransson, A., Chierici, M., Nomura, D., Granskog, M. A., Kristiansen, S., Martma, T., et al. (2020). Influence of glacial water and carbonate minerals on wintertime sea-ice biogeochemistry and the CO<sub>2</sub> system in an Arctic fjord in Svalbard. *Ann. Glaciol.* 61 (83), 320–340. doi: 10.1017/aog.2020.52
- Fransson, A., Chierici, M., Hop, H., Findlay, H., Wold, A., and Kristiansen, S. (2016). Late winter-to-summer change in ocean acidification state in Kongsfjorden, with implications for calcifying organisms. *Polar Biol.* , 1–17. doi: 10.1007/s00300-016-1955-5
- Frigstad, H., Andersen, T., Bellerby, R. G. J., Silyakova, A., and Hessen, D. O. (2014). Variation in the seston C:N ratio of the Arctic Ocean and pan-Arctic shelves. *J. Mar. Sys.* 129, 214–2230. doi: 10.1016/j.jmarsys.2013.06.004
- Gjelstrup, V. B. C., Sejr, M. K., de Steur, L., Christiansen, J. S., Granskog, M. A., Koch, B. P., et al. (2022). Vertical redistribution of principle water masses on the Northeast Greenland Shelf. *Nat. Comm.* 13, 7660. doi: 10.1038/s41467-022-35413-z
- Halbach, L., Vihtakari, M. P., Duarte, P., Everett, A., Granskog, M. A., Hop, H., et al. (2019). Tidewater glaciers and bedrock characteristics control the phytoplankton growth environment in an Arctic fjord. *Front. Mar. Sci.* 6. doi: 10.3389/fmars.2019.00254
- Hansen, H. P., and Koroleff, F. (1999). *Determination of nutrients, in Methods of Seawater Analysis. 3rd ed.* Eds. K. Grasshoff, K. Kremling and M. Ehrhardt (Weinheim, Germany: Wiley-VCH), 159–228. doi: 10.1002/9783527613984.ch10
- Henson, H. C., Holding, J. M., Meire, L., Rysgaard, S., Stedmon, C. A., Stuart-Lee, A., et al. (2022). Coastal freshening drives acidification state in Greenland fjords. *Sci. Total Environ.* 855 (2023), 158962. doi: 10.1016/j.scitotenv.2022.158962
- Hopwood, M. J., Carroll, D., Dunse, T., Hodson, A., Holding, J. M., and Iriarte, J. L. (2020). Review Article: How does glacier discharge affect marine biogeochemistry and primary production in the Arctic? *Cryosphere* 14, 1347–1383. doi: 10.5194/tc-14-1347-2020
- Jones, E., Renner, A., Chierici, M., Wiedmann, I., Biuw, M., and Lødemel, H. H. (2020). Seasonal dynamics of carbonate chemistry, nutrients and CO<sub>2</sub> uptake in a sub-Arctic fjord. *Elementa Sci. Anth.* 8 (1), 41. doi: 10.1525/elementa.438
- Johnson, K.M., King, A.E., and McN Sieburth, J. (1985). Coulometric TCO<sub>2</sub> analyses for marine studies; an introduction. *Marine Chemistry* 16 (1), 61–82.
- Joughin, I., Fahnestock, M., MacAyeal, D., Bamber, J. L., and Gogineni, P. (2001). Observation and analysis of ice flow in the largest Greenland ice stream. *J. Geophys. Res.* 106 (D24), 34021–34034. doi: 10.1029/2001JD900087
- Khan, S. A., Kjør, K. H., Bevis, M., Bamber, J. L., Wahr, J., Kjeldsen, K. K., et al. (2014). Sustain mass loss of the northeast Greenland ice sheet triggered by regional warming. *Nat. Climate Change* 4, 292–299. doi: 10.1038/NCLIMATE2161
- Ko, Y. H., Lee, K., Eom, K. H., and Han, I. S. (2016). Organic alkalinity produced by phytoplankton and its effect on the computation of ocean carbon parameters. *Limnol. Oceanogr.* 61, 1462–1471. doi: 10.1002/LNO.10309
- Krisch, S., Hopwood, M. J., Schaffer, J., Al-Hashem, A., Höfer, J., Rutgers van der Loeff, M. M., et al. (2021). The 79°N Glacier cavity modulates subglacial iron export to the NE Greenland Shelf. *Nat. Commun.* 12 (1), 3030. doi: 10.1038/s41467-021-23093-0
- Liang, H., Lyu, L.-N., Sun, C., Ding, H., Wurgaft, E., and Yang, G.-P. (2020). Low-molecular-weight organic acids as important factors impacting seawater acidification: A case study in the Jiaozhou Bay, China. *Sci. Total Environ.* 727 (2020), 138458. doi: 10.1016/j.scitotenv.2020.138458
- Lueker, T. J., Dickson, A. G., and Keeling, C. D. (2000). Ocean pCO<sub>2</sub> calculated from dissolved inorganic carbon, alkalinity, and equations for K<sub>1</sub> and K<sub>2</sub>: validation based on laboratory measurements of CO<sub>2</sub> in gas and seawater at equilibrium. *Mar. Chem.* 70, 105–119. doi: 10.1016/S0304-4203(00)00022-0
- Lydersen, C., Assmy, P., Falk-Petersen, S., Kohler, J., Kovacs, K. M., Reigstad, M., et al. (2014). The importance of tidewater glaciers for marine mammals and seabirds in Svalbard, Norway. *J. Mar. Sys.* 129, 452–471. doi: 10.1016/j.jmarsys.2013.09.006
- Macdonald, R. W., Carmack, E. C., McLaughlin, F. A., Falkner, K. K., and Swift, J. T. (1999). Connections among ice, runoff and atmospheric forcing in the Beaufort Gyre. *Geophys. Res. Lett.* 26, 2223–2226. doi: 10.1029/1999GL900508
- Manno, C., Bednaršek, N., Tarling, G. A., Peck, V. L., Comeau, S., Adhikari, D., et al. (2017). Shelled pteropods in peril: Assessing vulnerability in a high CO<sub>2</sub> ocean. *Earth-Space Rev.* 169, 132–145. doi: 10.1016/j.earscirev.2017.04.005
- Mattsdotter-Bjørk, M., Fransson, A., Torstensson, A., and Chierici, M. (2014). Ocean acidification state in western Antarctic surface waters: controls and interannual variability. *Biogeosciences* 11, 57–73. doi: 10.5194/bg-11-57-2014
- Mayer, C., Reeh, N., Jung-Rothenhäusler, F., Huybrechts, P., and Oerter, H. (2000). The subglacial cavity and implied dynamics under Nioghalvfjædsfjorden Glacier, NE-Greenland. *Geophys. Res. Lett.* 27 (15), 2289–2292. doi: 10.1029/2000GL011514
- Mehrbach, C., Culbertson, C. H., Hawley, J. E., and Pytkowicz, R. M. (1973). Measurement of the apparent dissociation constants of carbonic acid in seawater at atmospheric pressure. *Limnol. Oceanogr.* 18 (6), 897–907. doi: 10.4319/lo.1973.18.6.0897
- Meire, L., Søgaard, D. H., Mortensen, J., Meysman, F. J. R., Soetaert, K., Arendt, K. E., et al. (2015). Glacial meltwater and primary production as drivers for strong CO<sub>2</sub> uptake in fjord and coastal waters adjacent to the Greenland Ice Sheet. *Biogeosciences* 12 (8), 2347–2363. doi: 10.5194/bg-12-2347-2015
- Moon, T.A., Mankoff, K.D., Fausto, R.S., Fettweis, X., Loomis, B.D., Mote, T.L., et al. (2022). *Greenland Ice Sheet, Arctic Report Card* M.L. Druckenmiller, R.L. Thoman and T.A. Moon doi: 10.25923/c430-hb50
- Mucci, A. (1983). The solubility of calcite and aragonite in seawater at various salinities, temperatures and at one atmosphere pressure. *Am. J. Sci.* 283, 781–799. doi: 10.2475/ajs.283.7.780
- Nghiem, S. V., Hall, D. K., Mote, T. L., Tedesco, M., Albert, M. R., Keegan, K., et al. (2012). The extreme melt across the Greenland ice sheet in 2012. *Geophys. Res. Lett.* 39, L20502. doi: 10.1029/2012GL053611
- Niemi, A., Bednaršek, N., Michel, C., Feely, R. A., Williams, W., Azetsu-Scott, K., et al. (2021). Biological impact of ocean acidification in the Canadian Arctic: widespread severe pteropod shell dissolution in Amundsen Gulf. *Front. Mar. Sci.* 8. doi: 10.3389/fmars.2021.600184
- Orr, J. C., Epitalon, J.-M., Dickson, A. G., and Gattuso, J.-P. (2018). Routine uncertainty propagation for the marine carbon dioxide system. *Mar. Chem.* 207, 84–107. doi: 10.1016/j.marchem.2018.10.006
- Paulsen, M. L., Nielsen, S. E. B., Müller, O., Møller, E. F., Stedmon, C. A., Juul-Pedersen, T., et al. (2017). Carbon bioavailability in a high arctic fjord influenced by glacial meltwater, NE Greenland. *Front. Mar. Sci.* 4. doi: 10.3389/fmars.2017.00176
- Pierrot, D., Lewis, E., and Wallace, D. W. R. (2006). *MS Excel Program developed for CO<sub>2</sub> system calculations* (Oak Ridge, Tennessee: Carbon Dioxide Information Analysis Center, Oak Ridge National Laboratory, U.S. Department of Energy).
- Qi, D., Ouyang, Z., Chen, L., Wu, Y., Lei, R., Chen, B., et al. (2022). Climate change drives rapid decadal acidification in the Arctic Ocean from 1994 to 2020. *Science* 377, 1544–1550. doi: 10.1126/science.abo0383
- Redfield, A., Ketchum, B. H., and Richards, F. A. (1963). “The influence of organisms on the composition of sea water,” in *The Sea*, vol. 2. Ed. M. N. Hill (New York, USA: Interscience), 26–77.
- Rignot, E., Box, J. E., Burgess, E., and Hanna, E. (2008). Mass balance of the Greenland ice sheet from 1958 to 2007. *Geophys. Res. Lett.* 35, L20502. doi: 10.1029/2008GL035417
- Rignot, E., Koppes, M., and Velicogna, I. (2010). Rapid submarine melting of the calving faces of West Greenland glaciers. *Nat. Geosci.* 3, 187–191. doi: 10.1038/ngeo765

- Roy, R. N., Roy, L. N., Vogel, K. M., Porter-Moore, C., Pearson, T., Good, C. E., et al. (1993). The dissociation constants of carbonic acid in seawater at salinities 5 to 45 and temperatures 0 to 45°C. *Mar. Chem.* 44, 249–267. doi: 10.1016/0304-4203(93)90207-5
- Rysgaard, S. S., Glud, R. N., K. Lennert, K., Cooper, M., Halden, N., and Leakey, R. J. G. (2012). Ikaite crystals in melting sea ice—implications for pCO<sub>2</sub> and pH levels in Arctic surface waters. *Cryosphere* 6, 901–908. doi: 10.5194/tc-6-901-2012
- Sejr, M. K., Krause-Jensen, D., Rysgaard, S., Sørensen, L. L., Christensen, P. B., and Glud, R. N. (2011). Air–sea flux of CO<sub>2</sub> in arctic coastal waters influenced by glacial melt water and sea ice. *Tellus* 63B, 815–822. doi: 10.1111/j.1600-0889.2011.00540.x
- Spalding, C., Finnegan, S., and Fischer, W. W. (2017). Energetic costs of calcification under ocean acidification. *Global Biogeochem. Cycles* 31, 866–877. doi: 10.1002/2016GB005597
- Stedmon, C. A., Granskog, M. A., and Dodd, P. A. (2015). An approach to estimate the freshwater contribution from glacial melt and precipitation in East Greenland shelf waters using colored dissolved organic matter (CDOM). *J. Geophys. Res. Oceans* 120, 1107–1117. doi: 10.1002/2014JC010501
- Straneo, F., Hamilton, G. S., Sutherland, D. A., Stearns, L. A., Davidson, F., Hammill, M. O., et al. (2010). Rapid circulation of warm subtropical waters in a major glacial fjord in East Greenland. *Nat. Geosci.* 3, 182–186. doi: 10.1038/NGEO764
- Sulpis, O., Lauvset, S. K., and Hagens, M. (2020). Current estimates of K<sub>1</sub>\* and K<sub>2</sub>\* appear inconsistent with measured CO<sub>2</sub> system parameters in cold oceanic regions. *Ocean Sci.* 16, 847–862. doi: 10.5194/os-16-847-2020
- Tanioka, T., Garcia, C. A., Larkin, A. A., Garcia, N. S., Fagan, A. J., and Martiny, A. C. (2022). Global patterns and predictors of C:N:P in marine ecosystems. 2022. *Commun. Earth Environ.* 3, 271. doi: 10.1038/s43247-022-00603-6
- Thomsen, H. H., Reeh, N., Olesen, O. B., Boggild, C. E., Starzer, W., Weidick, A., et al. (1997). The Nioghalvfjærdssjorden glacier project, North-East Greenland: a study of ice sheet response to climatic change. *Geol. Greenland Survey Bull. GEUS* 176, 95–103. doi: 10.34194/GGUB.V176.5073
- Treguer, P., Nelson, D. M., Gueneley, S., Zeyons, C., Morvan, J., and Buma, A. (1990). The distribution of biogenic and lithogenic silica and the composition of particulate organic matter in the Scotia Sea and the Drake Passage during autumn 1987. *Deep-Sea Res.* 37, 833–851. doi: 10.1016/0198-0149(90)90009-K
- Turk, D., Bedard, J. M., Burt, W. J., Vagle, S., Thomas, H., Azetsu-Scott, K., et al. (2016). Inorganic carbon in a high latitude estuary-fjord system in Canada's eastern Arctic Estuar. *Coast. Shelf Sci.* 178 (2016), 137–147. doi: 10.1016/j.ecss.2016.06.006
- von Albedyll, L., Schaffer, J., and Kanzow, T. (2021). Ocean variability at Greenland's largest glacier tongue linked to continental shelf circulation. *J. Geophys. Res. Oceans* 126, 1–15, e2020JC017080. doi: 10.1029/2020JC017080
- Wanninkhof, R. (2014). Relationship between wind speed and gas exchange over the ocean revisited. *Limnol. Oceanogr. Methods* 12, 351–362. doi: 10.4319/lom.2014.12.351
- Yamamoto-Kawai, M., McLaughlin, F. A., Carmack, E. C., Nishino, S., and Shimada, K. (2009). Aragonite undersaturation in the arctic ocean: effects of ocean acidification and sea ice melt. *Science* 326, 1098–1100. doi: 10.1126/science.1174190